SURFACE-ACTIVE NANOPLATE FOR OIL RECOVERY

A Dissertation

by

LECHENG ZHANG

Submitted to the Office of Graduate and Professional Studies of
Texas A&M University
in partial fulfillment of the requirements for the degree of

DOCTOR OF PHILOSOPHY

Chair of Committee,	Zhengdong Cheng
Committee Members,	Mustafa Akbulut
	A. Daniel Hill
	Qingsheng Wang
Head of Department,	M. Nazmul Karim

May 2020

Major Subject: Chemical Engineering

ABSTRACT

Janus colloidal surfactants with opposing wettability on two structural parts are receiving attention for their intriguing structural and practical application in various industries. Combining the advantages of molecular surfactants and particle-stabilized Pickering emulsions, Janus colloidal surfactants generate remarkably stable emulsions. This dissertation developed a straightforward and cost-efficient strategy to develop Janus nanoplate surfactants (JNPS) from aluminosilicate nanoclays materials, including Kaoinite and Halloysite, by stepwise surface modifications, including an innovative selective surface modification step. Such colloidal surfactants are found to be able to stabilize Pickering emulsions of different oil/water systems. The microstructural characterization of solidified polystyrene emulsions indicates that the emulsion interface is evenly covered by JNPS. The phase behaviors of water/oil emulsion generated by these novel platelet surfactants were also investigated. Furthermore, this dissertation demonstrated the application of JNPS for enhanced oil recovery with a microfluidic flooding test, showing a dramatic increase of oil recovery ratio. This research provides important insights for the design and synthesis of two-dimensional Janus colloidal surfactants, which could be utilized in biomedical, food and mining industries, especially for circumstances where high salinity and high temperature are involved.

ACKNOWLEDGEMENTS

I would like to express my gratitude to my committee chair, Dr. Zhengdong Cheng and my committee members, Dr. Hill, Dr. Akbulut, Dr. Wang and Dr. Mannan for your guidance, suggestions and encouragement throughout the course of this research.

My sincere thanks also go to my friends and the department staff for making my time at Texas A&M University a great experience.

I would like to dedicate my dissertation to my parents Wenjuan Song and Ligang Zhang, and my beloved wife Tailynn Dinh for their love, encouragement and endless support.

CONTRIBUTORS AND FUNDING SOURCES

Contributors

This work was supervised by dissertation committee consisting of Dr. Zhengdong Cheng [advisor] and Dr. Mustafa Akbulut and Dr. Qingsheng Wang of the Department of Chemical Engineering and Professor Dr. Dan Hill of the Department of Petroleum Engineering.

I complete this research work by collaborating and discussing with my fellow coworkers, including Dr. Mingxiang Zeng, Mr. Dali Huang, Dr. Xuezhen Wang, Mr. Abhijeet Shinde and Dr. Ling Wang.

Funding Sources

Research work in this dissertation is funded by PetroChina Scientific Research and Technology Development Project (2014A-1001-01), Texas A&M Water Seed Grant (28-163024-00001), Texas A&M Aggie Challenge Program at different stage. The authored is also supported by Mary Kay O'Connor Process Safety Center in the last two years of my study.

NOMENCLATURE

JNPS	Janus Nanoplate Surfactants
GQD	Graphene Quantum Dots
ATRP	Atom Transfer Radical Polymerization
NIPAM	N-Isopropylacrylamide
PMDTA	Pentamethyldiethylenetriamine
DIW	Deionized Water
PPA	Phenyl Phosphonic Acid
si-ATRP	Surface-Initiated Atomic Transfer Radical Polymerization
APTES	3-Aminopropyl Triethoxysilane
TEA	Triethylamine
BiBB	Bromo-Isobutyryl Bromide
DMAEMA	Dimethylamino Ethyl methacrylate
ETBriB	Ethyl Bromoisobutyrate
CuCl	Copper Monochloride
DCM	Dichloromethane
AIBN	Azobisisobutyronitrile
FT-IR	Fourier-transform infrared spectroscopy
ssNMR	Solid-state nuclear magnetic resonance
SEM	Scanning electron microscopy
TEM	Transmission electron microscopy
VES	Visco-Elastic surfactant

LPG	Liquefied petroleum gas
HPGG	Hydroxypropyl Guar Gum
IFT	Interfacial tension

TABLE OF CONTENTS

Page

LIST OF FIGURES

Page

LIST OF TABLES

Page

CHAPTER I

INTRODUCTION*

1.1. Research Background

The injection of nanofluids into oil reserviors, a novel chemical enhanced oil recovery(EOR) technique, has the potential to produce a greater portion of the 50% of in-place oil reserves, which is currently not recoverable by conventional primary and secondary recovery methods [1,2], nor even by conventional EOR, such as polymer or surfactant flooding. Nanotechnology and nanomaterials, which have garnered attention in the upstream industry [2,3], may enable greater recovery ratios from oil bank reserves [3-5]. Nanofluid flooding, also called Nanoflooding, is a new chemical EOR technique whereby nanomaterial or nanocomposite fluids are injected into oil reservoirs to effect oil displacement or to improve injectivity [6]. Current EOR techniques comprise chemical, thermal, microbial, miscible gas, and immiscible gas techniques. In particular, chemical EOR, involving the use of polymers, surfactants, or alkali to improve sweep efficiency and oil displacement, enjoys a proven history of successful applications in reducing oil production cost, increasing efficiency, and stimulating oil well productivity [7]. The recovery percentage of conventional chemical EOR techniques, however, is unable to recover roughly 50% of oil reserves [8]. Considering current low oil prices, technology innovation could increase production from existing assets and moderate the effect of shrinking profit margin. This section will review technology innovations, like

* Reproduced from Reference 125 with permission from the Royal Society of Chemistry.

nanoflooding, to help both academia and upstream industry to grasp the trending of nanoflooding clearly. Compared with conventional chemical flooding, nanofluid flooding has several advantages. By modifying material surface functionalization or altering template materials, engineered nanomaterials can possess additional functions, such as magnetic-responsive and pH-responsive properties. In addition, the unique functions of nanomaterials allow nanofluid to recover those inaccessible oil reserves using conventional methods. Finally, different from molecular surfactant or polymer stabilized emulsions, nanoparticle-stabilized emulsions, also known as Pickering emulsions, are very stable even under harsh reservoir conditions, owing to the well-organized particle layer at the emulsion interface.

Some previous reviews have summarized applications of nanotechnology in enhanced oil recovery from the petroleum engineering perspective [1,5,6, 9]. Shamsi Jazeyi *et al.* gave a thorough discussion on application of polymer-coated nanoparticles in enhanced oil recovery [10]. In this Chapter, I will discuss nanoflooding techniques from the material and colloidal science perspective, focus on the fundamental mechanisms underlying the nanofluid enhanced oil recovery and parameters controlling the success of a nanoflooding operation. Potential functions of nanomaterials in nanofloodings proposed by researchers will be reviewed first to explain two questions: what are the advantages and limitations of nanofluid flooding techniques and what is the potential mechanism of nanofluid flooding. Then, I will summarize current nanomaterials, which have been tested for nanoflooding EOR. This dissertation will be based on three categories of material dimensions: zero-dimensional nanostructures (nanoparticles and heteroepitaxial core-shell structures), one-

dimensional nanostructures (nanorods, nanowires, and nanotubes), and two-dimensional structure (thin plates, sheets). I will also summarize data to compare performance of nanofloodings with different materials under each category. Next, I will outline factors that can affect nanoflooding quality, such as particle morphology, surface decoration, and particle environment resistance, to illustrate how to enhance oil recovery by nanofluid and how to mitigate risks associated with nanofluid flooding. With the advantages of small size and different geometries, different dimensions of nanoparticles can achieve free movement in suitable oil reservoirs of different permeabilities. However, particle morphology and surface decoration of nanomaterials not only affect particle retention in the formation but also change emulsion stability. Different knowledges on the nanomaterial structures and morphologies, surface decorations and emulsion stabilizations can help engineers and scientist to implement nanofloodings in a more successful way. Finally, I will discuss the potential opportunities and challenges of nanomaterial-assisted EOR.

1.2. Functions of Nanomaterials in Nanofloodings

1.2.1. Wettability Alteration

Wettability alteration is a well-known practice for conventional surfactant flooding [11,12], especially for carbonate formation which is typically oil-wet and mix–wet. Spontaneous water imbibition is constrained under these formation conditions, resulting poor recovery ratio with waterflooding method. Different from waterflooding method, surfactant flooding changes formation wettability, hence, it decreases capillary force and enhance the mobility of the oil phase. The general mechanism of wettability alteration

with conventional molecular surfactant has been well studied and reported by different literatures [13-15]. The common explanation is surfactants interact and absorb on the rock surfaces to change wettability. Another possible mechanism is natural lyophilic surfactant generated by crude oil oxidization is removed by ion pairs, thus surface wettability turns to hydrophilic.

For nanofloodings, wettability alteration mechanism is slightly different. As material size reduces to nanometer range, its property becomes different from bulk material exhibiting unique applications. A good example will be that compared with bulk material, the small size of nanomaterials increases its total surface area in several orders of magnitude. The large surface area ratio increase the possibility for nanosurfactant to be adsorbed on rock surface and also improve the adherence of surfactant [16].

Karimi *et al.*[12] observed wettability alteration in carbonates surface with zirconium oxide nanofluid (shown in Figure 1). With microscopic imaging and theoretical calculation, he proposed that the wettability alteration is due to ZrO_2 deposition on the rock surface and governed by the partition coefficient of nanomaterial in water and oil phases. Their result also shows the wettability alteration by nanofluid is a slow process that may take days to finish. Other researchers proposed to use surface-modified material for wettability alteration. Recently, Luo et al.[17] reported “climbing film”, which is an assembly of surface-modified Janus graphene nanosheets that serve to reverse wettability of solid surfaces, shown in Figure 2. The same wettability alterations by nanoparticles and the nanoparticle mixture were also reported by Giraldo *et al.*[18], Maghzi *et al.*[19] and Dehghan Monfared *et al.*[11]. According to above literatures, wettability alteration can be

affected by particle size, co-surfactants, pH value, and ion strength[10]. We have also noticed that some researchers claimed SiO_2 nanoparticles can also be applied as an augmented injection agent. The mechanism for depression and augmented injection is also very similar to the wettability alteration [20,21].

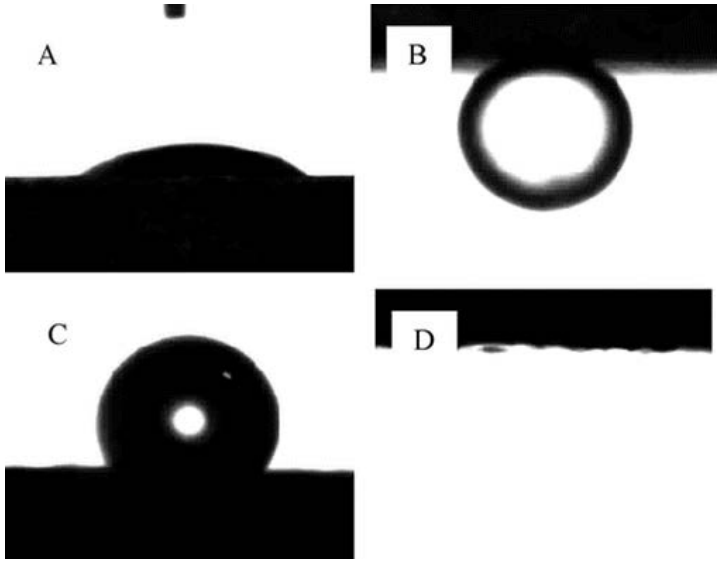

Figure 1. Wetting conditions for rock surface in different phases ((A) air/water, (B) water/n-heptane) and a carbonate rock aged in the oil ((C) air/water, (D) water/n-heptane).(Reprinted with permission from [12]. Copyright (2012) American Chemical Society.)

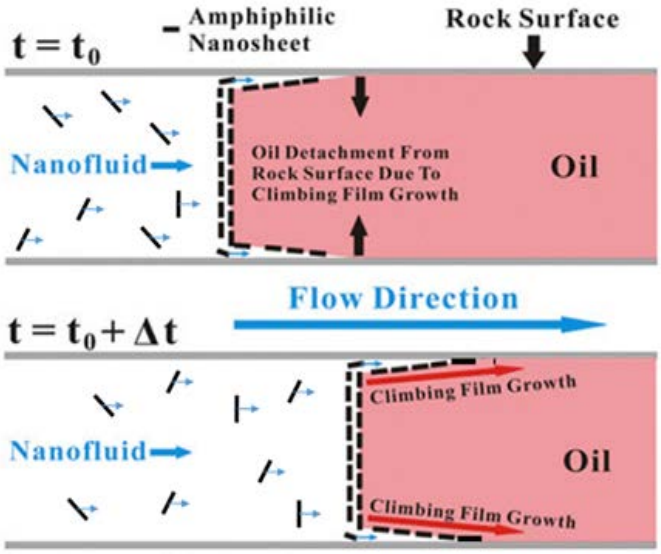

Figure 2. Oil displacement mechanism proposed by Luo et al. (Figure adapted from [17]. Reprint permission is waived by PNAS for educational use.)

1.2.2. Reduction of Interfacial Tension

Interfacial tension (IFT) is an important concept in surface science, which can be understand as energy change per surface area. When two immiscible liquids are mixed, the interface between two phases will tend to reduce to keep total interfacial energy at minimum. When surface active chemical is added into immiscible phases, the amphiphilic structure of surfactant can reduce interfacial tension between two phases, as a result, even total interface area increases during emulsification, total surface energy will still be relatively low. Hence, a stable homogenous emulsion can be formed.

$$\gamma = \frac{W}{\Delta A} = \frac{F \cdot \Delta x}{2 \cdot L \cdot \Delta x} = \frac{F}{2L}$$

To increase oil recovery ratio, one of the common strategies is to reduce the oil-water interfacial tension. For conventional surfactant flooding, interfacial tension is a

standard parameter to be used for surfactant characterization. The lowest oil-water interfacial tension by molecular surfactant can reach 10^{-3}-10^{-2} mN/m [22,23].

Common nanofluid systems does not possess amphiphilic structure, thus it cannot reduce interfacial tension. Common nanofluid systems cannot achieve small interfacial values like molecular surfactant, researchers had tried different method to reduce interfacial tension between oil and water by nanomaterials [24, 25, 26]. The most common method is through surface-modification or asymmetrical surface-modification. When nanoparticles or nanoplatelets are modified with hydrophobic and hydrophilic groups on opposite sides, it creates a Janus particle (named by Nobel Laureate P.G. de Gennes [27]), then the particle has the potential to reduce interfacial tension (IFT) sharply. The surface activity of Janus particle is dependent on its surface modifications. To use Janus particles as active surfactants, each side of the particle must exhibit distinctive surface hydrophilicity [28]. More detail will be discussed in the surface modification section later.

1.2.3. Controllable Viscosity

Another important dimensionless number in EOR is mobility ratio, which is the ratio between the displacing fluid and displaced fluid. A higher mobility ratio is desired for more oil displacement, under which has a higher sweep efficiency and less fingering effect in the reserve [22]. Nanofluids have been reported to be used to reduce oil viscosity and increase displacing fluid viscosity. Both factors will contribute to increase mobility ratio and as a result, boost oil recovery ratio [29].

1.2.4. Disjoint Pressure for Oil Displacement

A disjoining pressure at the oil-water-solid contact region has been observed and studied during nanoflooding, which is one of the driving forces to expel oil from rock surface [30,31]. The pressure magnitude is related with wedge film thickness and nanoparticle structure and can be theoretically calculated (Figure 3) [32]. Recently Zhang *et al.* [33] displayed their work on crude oil displacement with nanofluid. They concluded that disjoining pressure is the mechanism underlying their successful oil displacement with sandstone experiment.

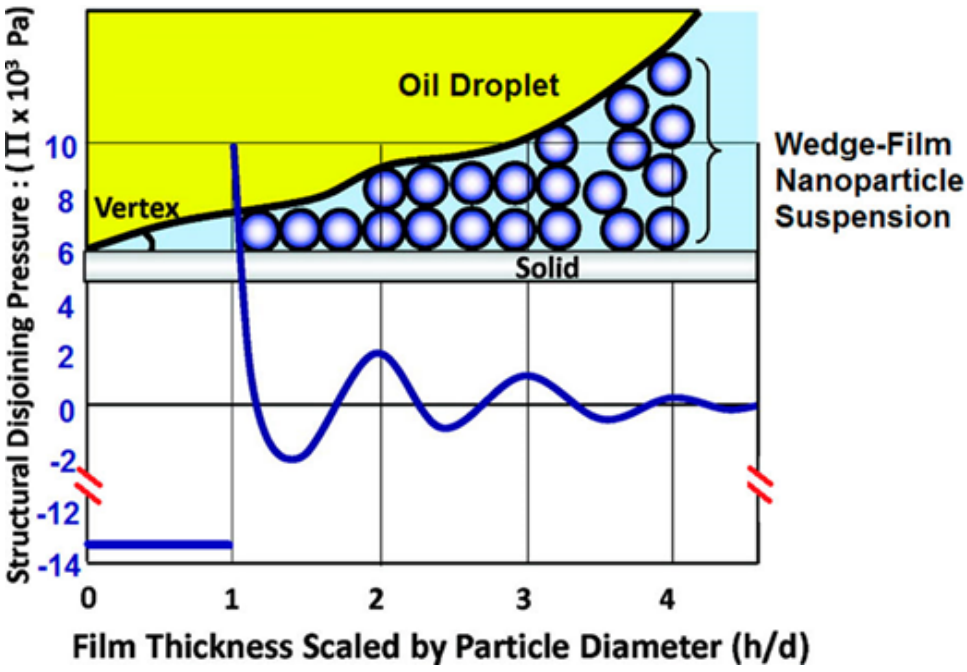

Figure 3. Schemetic shows nanoparticle wedge film confined by solid surface and oil-nanofluid interface and relationship between disjoining pressure and film thickness. (Reprinted with permission from [33]. Copyright (2014) American Chemical Society.)

1.2.5. Stable Foam and Emulsion under Harsh Conditions

Harsh conditions, i.e. high temperature, high pressure and high salinity, are always challenges for conventional molecular surfactant flooding because under harsh conditions,

molecular surfactant may undergo phase separation and render the surfactant solution into inhomogeneous phases [34]. Nanoparticles and surface-modified nanoparticles, on the other hand, have been reported with high thermal stability and been analyzed with flooding experiment in laboratory [35,36]. Moreover, foam stability and emulsion stabilization are important for conducting flooding for reservoirs with harsh conditions. Pickering emulsion and Pickering foam have shown stability under extreme conditions [37,38]. Thermal stability would be another merit that nanoparticles can contribute to the flooding procedure. Stabilization of Pickering emulsions can be controlled by manipulating particle morphology and surface modification. Synthesis of anisotropic particles have been reported previously [39-41]. Stable foam or emulsion is necessary for emulsion or foam flooding. From the perspective of thermal dynamics, reserved oil bank will tend to become emulsified and mobilized if the emulsified oil can form stable emulsions, thereby increasing oil recovery ratio. A major application of surface modified nanoparticles, therefore, is stabilization of emulsions and foams [42]. Zhang *et al.* applied silica nanospheres that have been surface-modified with PEG on foams and emulsions to promote conformance [38,43]. Meanwhile, hydrophobic silica particles stabilized water/CO_2 emulsion was firstly reported by Adkins *et al.*[44]. Emulsion ripening and coalescence is not obvious, however, the author concluded that particle sedimentation is the major contribution for destabilization. Later, Janus particles are reported to be used for CO_2 flooding, a popular technique for EOR in areas where CO_2 can be easily achieved [45,46]. Guo *et al.* studied silica and clay stabilized CO_2 foam structure and its EOR applications.

They demonstrated that CO_2 foam is improved by the nanoparticle and surfactant mixture[47].

1.3. Nanomaterials for Nanoflooding

The geometry of nanomaterial can affect its functionality, especially in anisotropic material such as Janus particles. This section will review the applications of nanomaterials with different geometries for enhanced oil recovery. To categorize nanomaterial with different geometry, the nanomaterial dimension number is used. The dimension number is defined by the number of dimensions that are not within nanoscale (100 nm).

1.3.1. Zero-dimensional Nanomaterials (Such as, Nanoparticles and Quantum Dots)

In this section, I will review several laboratory experiments investigating the use of zero-dimensional nanomaterials, such as quantum dots and nanoparticles, for oil recovery. Oil recovery ratio with zero-dimensional nanoparticles will also be discussed here. Silica dioxide, among other zero-dimensional materials, has been used to increase oil recovery ratio. To study oil sweep efficiency of silica particles under different conditions, Skauge *et al.*[48] conducted experiments on hydrophilic silica nanoparticles and compared the result with polystyrene nanoparticles. Results show that silica particles possess a low differential pressure and small permeability reduction. With further investigation, Skauge found when system combined with brine or with a 300-ppm polymer solution, there is no significant oil mobilization; however, if applied with a 600-ppm polymer solution which has a higher viscosity, the oil bank can be mobilized. Author explained this result with silica particles being “log-jammed” at the pore throat, thus

requiring a high viscosity to generate the oil bank during microscopic observation. Hendraningrat *et al.* also studied zero-dimensional nanoparticles sweep efficiency with glass microchannels and microchips (shown in Figure 4). He found that 0.1 wt% silica particles flooding can achieve higher oil recovery ratio compared to the brine control group [49]. Researchers have also tried other zero-dimensional nanoparticles than silica for enhanced oil recovery. Ogolo *et al.*[29] tested nanoparticles other than silicon dioxide, such as aluminum oxide and magnesium oxide, with different solvents. In these trials, aluminum oxide with distilled water achieved the most successful flooding result. This solution delivered 12.5% more on oil recovery ratio than slick water flooding.

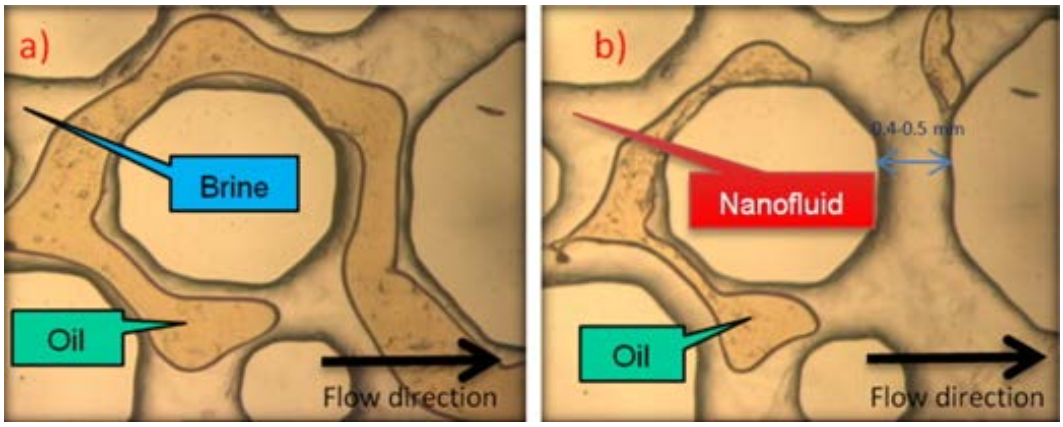

Figure 4. Flooding experiment carried out with microfluidic chip (a) brine flooding (b) silica particle nanoflooding. Hendraningrat et al. concluded that nanofluid can potentially increase recovery rate. (Reprinted with permission from [49]. Copyright (2013) Elsevier.)

Another category of zero-dimension material used in the oil field is nanocapsule. The encapsulated breaker has already been used in hydraulic fracturing to reduce the viscosity of cross-linked systems [50]. Some researchers also proposed to use encapsulated self-healing polymers for storage tank and pipeline self-repair [51]. The use of

nanoencapsulation for enhanced oil recovery have been proposed in Bennetzen's paper [52]. In the paper, Bennetzen mentioned that fluorescent encapsulate can be used as a tracer to differentiate different reservoir conditions, such as pH value, temperature, oil water content and salinity. Also, nanocapsules can be used to deliver chemicals to specific regions then triggered to release chemicals.

1.3.2. One-dimensional Nanomaterial (Such as, Nanofibers and Nanowires)

Because of its natural abundance and accessibility, many one-dimensional nanofibers and nanotubes have been examined for oil recovery and oil emulsification. The one of the most popular one-dimensional nanofiber is carbon nanotubes. Several researchers reported that carbon nanotubes demonstrated superoleophilicity and can be applied in oil/water emulsion stabilization. Hu *et al.* demonstrated, by grafting one-dimensional Carbon Nanotube (CNTs) onto functionalized graphene aerogel surface, the aerogel shows superhydrophobicity and oleophilicity. The capacity and selectivity can also be fine-tuned by pore size and channel diameter [53]. Zhai *et al.* reported silver phosphate and multiwall carbon nanotube-stabilized Pickering emulsion for photo catalysis use [54]. Shen *et al.* used carbon nanotube/silica nanohybrids to stabilize decalin and showed controllable emulsion type and volume fraction with different particle concentrations [55]. Applying synthetic amphiphilic nanorods for EOR may increase the cost of production. A more feasible and cost-effective solution is applying natural material. Kusanagi *et al.* reported core flooding results with cellulose nanofibers. To control fluid mobility, 0.4 wt% cellulose nanofiber and corsslinker $AlCl_3$ were injected into an inhomogeneous core sample. The crosslinked cellulose fiber was able to control mobility

of nanofluid and increase recovery ratio from 13.3% to 24.3%; however, severe filtration was also observed during experiment [56]. Titanium dioxide nanoparticles and nanorods have been used in nanofloodings. Ehtesabi *et al.*[57] applied anatase and amorphous titanium dioxide in core flooding test and they found oil recovery ratio increased to 80% compared to the value for pure water flooding 49%. With further testing, they concluded that the reason of increasing oil recovery ratio is rock wettability change by the nanorods. Some papers reported using low-cost natural one-dimensional material to stabilize emulsions. Kalashnikova *et al.* reported hexane/water emulsion stabilized by bacterial cellulose nanocrystals, nanofibers from cotton, and other natural nanofibers [58,59]. Nanofibers with different aspect ratios were utilized in their experiments. They found aspect ratio could influence emulsion surface coverage of nanofibers.

1.3.3. Two-dimensional Nanomaterial (Such as, Nanosheets and Nanoplatelets)

Variations in particle geometry can greatly change the properties of emulsions, including ability to reduce interfacial tension, emulsion and foam stabilization [60], which is essential for emulsion and foam flooding under harsh reservoir conditions. Numerical simulation work justified two-dimensional material is more favorable for emulsion stabilization when compared with zero-dimensional and one-dimensional materials.

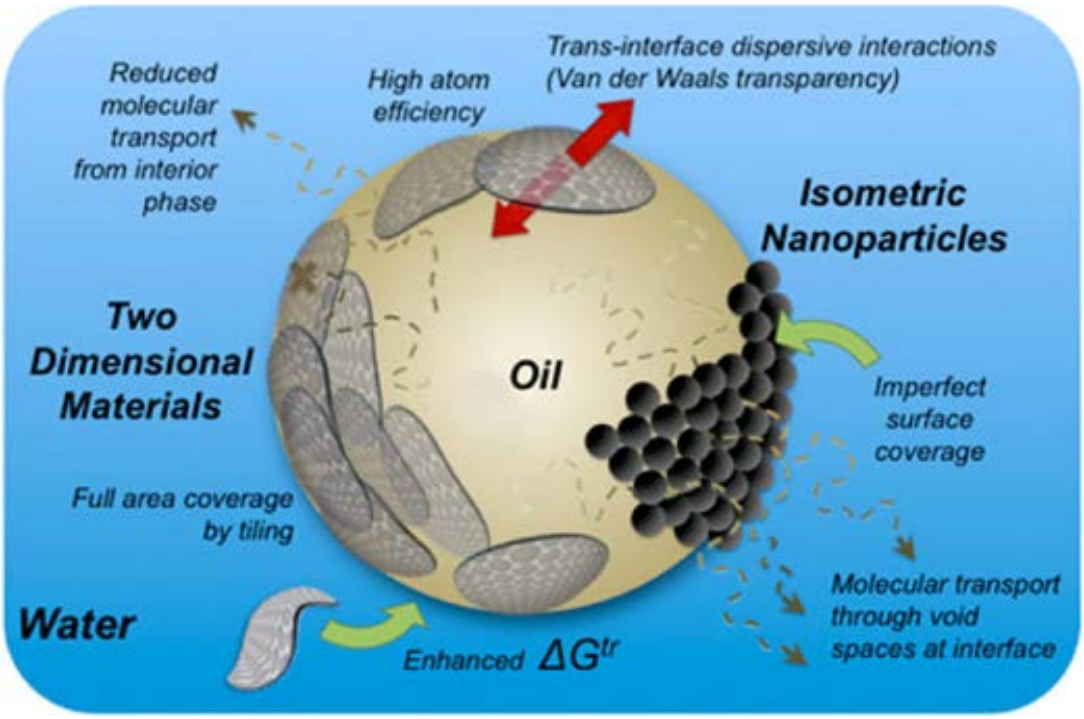

Figure 5. Schematic illustrates advantage of two-dimensional nanosheets over zero-dimensional nanoparticles to stabilize emulsions. (Reprinted with permission from [61]. Copyright (2014) American Chemical Society.)

Creighton *et al.*[61] presented a thermodynamic model to analyze the free energy change during particle stabilization, shown in Figure 5. Benefits of utilizing two-dimensional materials include: First, large surface area produces deeper energy trap, which enhances emulsion stability. Second, better coverage with two-dimensional material provides better coverage at interface, reducing the rate for emulsion coalescence. Last but not least, since material thickness is minimal compared to diameter, atom utilization efficiency for two-dimensional material is higher than other geometry, which could reduce the cost for application.

For two-dimensional thin film, the stabilization energy can be expressed as:

$$\Delta G = \pi R^2[\gamma_{o/w} - |\gamma_{o/s} - \gamma_{w/s}|] \quad \text{Equation.1}$$

where R is radius of disk, $\gamma_{o/w}$ is oil/water interfacial tension, $\gamma_{o/s}$ is oil/disk interfacial tension, and $\gamma_{w/s}$ is water/disk interfacial tension. Creighton *et al.* further developed the equation by applying Young's equation. Researcher found that the Gibbs energy change is related to emulsion droplet radius, interfacial tension, and three-phase contact angle. Many types of two-dimensional nanomaterials have been used to prepare emulsions. Graphene and graphene oxide are common carbon-based nanosheets. Kim *et al.*[62] reported amphiphilic graphene oxide sheet in 2010, shown in Figure 6. The amphiphilicity is due to the carboxylic group on the edge and to the hydrophobic basal surface. By changing pH value, dissociation of carboxylic varies, resulting a tunable amphiphilicity. Luo *et al.*[17] successfully modified a single face of graphene oxide and reported a 15.2% increase in oil recovery ratio. By applying modified graphene at the interface of oil and water, they generated an interfacial film with strong elasticity that exhibits special properties of a two-dimensional material.

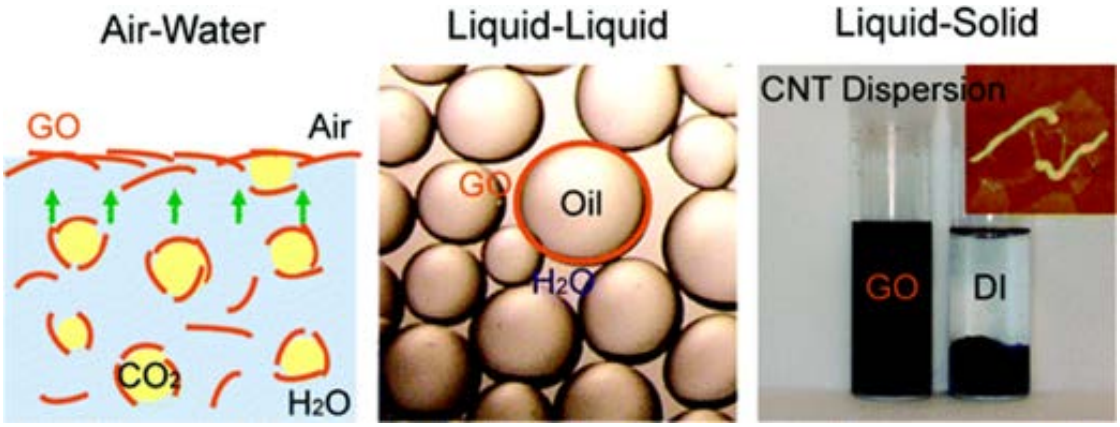

Figure 6. Amphiphilic graphene oxide between different interfaces. (Reprinted with permission from [62]. Copyright (2010) American Chemical Society.)

Other two-dimensional materials, especially low-cost natural clay disk materials, have also been modified and used as emulsifiers and foam stabilizers. Mejia *et al.*[63] modified zirconium phosphate surface with octadecyl isocyanate, then exfoliated the zirconium phosphate structure to generate Janus and Gemini platelets. Researcher also found that emulsion droplet size is related to particle concentration. Based on the modification method published by Mejia [63], Yu *et al.* varied surface functionalization groups. Using the 0.4 wt% modified zirconium phosphate nanoplatelet, they achieved 65% oil recovery ratio. In the same work, they also demonstrated synergetic effect between zirconium phosphate and molecular alkyl polyglycoside (APG) surfactant on enhanced oil recovery. Recovery ratio can increase to 80% with nanoplatelets/APG mixed surfactants[64]. Later, Wang *et al.*[65] used the Janus surfactant developed in Mejia's paper to encapsulate phase changing material (PCM), which is thermally stable and uniform in particle size. The successful application of Janus particle surfactant verified the functionality of Janus nanoplatelets for oil emulsification. Guillot *et al.* studied laponite and montmorillonite behavior at the water/oil interface [66].According to their publication, in some trials, although the montmorillonite plate sizes are larger than emulsion droplets, the plates wrap around the emulsion droplets to stabilize them. Yang *et al.* found paraffin/water emulsion can be solely stabilized by layered double hydroxide. They proposed the mechanism of stabilization is due to reduction of zeta potential [67]. Figure 7 shows oil phases stabilized by different dimensions of nanomaterials.

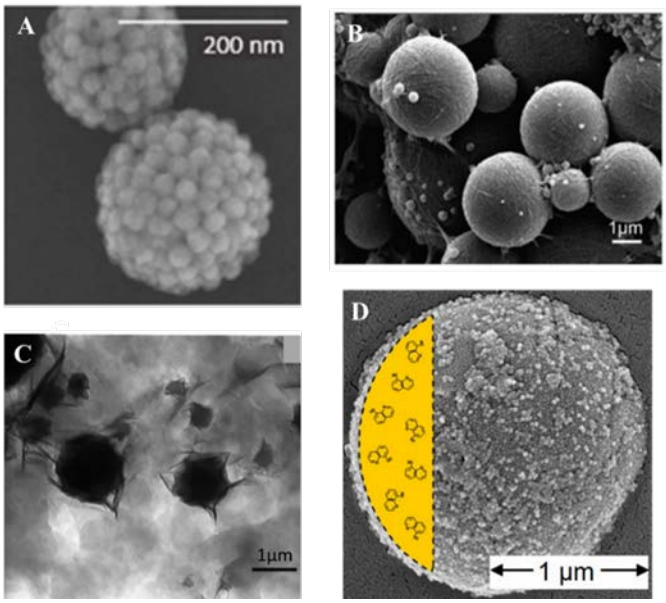

Figure 7. (a) Hydrophilic silica nanoparticles stabilized by inverse Pickering emulsion droplets (Reprinted with permission from[168], copyright (2015) American Chemical Society). (b) Polystyrene stabilized by bacteria cellulose nanofibers reported by Kalashnikova et al. (Reprinted with permission from[57]. Copyright (2011) American Chemical Society). (c) Polyacrylamide (PAAm) latex particles stabilized by surface modified montmorillonite. (Adapted with permission from[139]. Copyright (2006) American Chemical Society). (d) pH-sensitive encapsulates stabilized by silica particles reported by Haase et al. (Reprinted with permission from[69]. Copyright (2010) American Chemical Society).

Table 1 summarizes materials used for nanoflooding by different dimensions that are discussed in this paper.

Table 1. Examples of nanomaterial with different morphologies being apploed in nanoflooding for EOR

Dimension	Material	Research Examples
Zero-dimensional	Silica; surface-modified silica; silica hybrids; silica dumbbell; aluminum oxide; magnesium oxide;	[29,42,48,68,69]
One-dimensional	Carbon nanotubes; bacterial cellulose nanocrystals; cotton nanofibers	[54-56,58,59]
Two-dimensional	Graphene; graphene oxide; clay materials	[17,62,63]

1.4. Factors Controlling Success of Nanoflooding

After review results obtained from laboratories, it appears that nanofloodings techniques could have advantages over conventional flooding techniques at oil emulsification, wettability alteration and foam stabilization, and they possess unique mechanisms for oil displacement [6,11,18,28]. Moreover, modification of material structure and morphology can further enhance material performance for nanoflooding. Following are several factors that can be adjusted to improve nanoflooding quality:

1.4.1. Nanomaterial Structure

A major concern of applying lamellar nanoparticles in EOR is material swelling , thus causing formation jamming and formation damage[70] especially for unmodified clay nanomaterials with layered structures which can be intercalated with formation water. After interacting with water, exchangeable ions within the clay structure will hydrate and

expand the d-space of layered clay material. A 60% to 380% increase in d-space has been observed, which is the root cause for severe formation damage[71]. Applying swelling inhibitors (like K^+) or using exfoliated clay materials[71-73] can mitigate material swelling issues and thus solve the formation damage problem. Gonzalez *et al.* reported applying swelling inhibitors can achieve a swelling reduction up to 60% [74]. Exfoliation and delamination of different lamellar clay materials have been well studied in laboratory [75, 76, 77]. The application of exfoliated clay can fundamentally resolve the swelling issue since the exfoliated clay only consists of a single layer of crystal cell, so the layered structure no longer exist.

1.4.2. Nanomaterial Morphology

Physical size of the pore throat will place a physical limitation on the success of nanoparticle-assisted EOR, thus right morphology is an important criterion for successful nanoflooding operation. If the physical size of nanomaterial is larger than the pore throat, then materials cannot propagate through the pore neck, which will hinder material function. Even worse, formation damage is possible due to pluggage. In some cases, although the size of individual particles is smaller than pore throat size, the materials still cannot pass through the pore neck due to the log-jamming phenomenon [6]. Particle retention and entrapment are the main causes of log jamming [49,78]. To prevent potential formation damage, first particle size has to be controlled to let material pass through the throat neck freely. Meanwhile, particle hydrophobicity, fluid ion strength, and formation conditions should also be considered and modified to avoid jamming. The ratio of particle size to pore size and fluid velocity are two other factors controlling retention and

entrapment [79]. Different papers have discussed nanoparticle entrapment theoretically and experimentally [80,81]. According to the analysis in the above papers, particle retention, therefore, is related to particle morphology and physical size.

Nanoparticle shape and morphology can also play an important role in oil emulsification, as evidenced by interests in particle-stabilized emulsions, also known as Pickering emulsions [82]. Interface stability is related to surface wettability, aspect ratio, and especially to particle shape. De Folter *et al.* reported Pickering emulsions with cubic and peanut-shaped particles achieved 90% surface coverage, higher than that achieved with normal spherical particles [83]. Gao *et al.* numerically studied surface activity of different shapes of Janus particles and found sphere and rod shapes have only one equilibrium state. According to his report, compared to other material morphology, discotic shapes have another energy state, reverse orientation state. This energy state will enable discotic shape particle stabilized emulsion stays at lower energy state to increase emulsion stability [60]. Madivala *et al.* observed a strong correlation between particle aspect ratio and emulsion stability [84]. In this study, author proved with experiments that for non-spherical particles, such as rods, there is a critical aspect ratio, if the particle aspect ratio is above the critical value, then a stable emulsion can be generated with little energy and low particle consumption. Above examples demonstrated that particle morphology parameters, such as aspect ratio, can greatly affect emulsion stability and emulsification energy.

1.4.3. Formation Salinity, Temperature and pH Value

Formation salinity, temperature, and pH value can impact nanoflooding performance, and inorganic material stability can be affected by those variables. Before

implementing nanomaterial for flooding, compatibility of nanomaterials with formation conditions, such as formation salinity, temperature and pH value. McElfresh's recent research examined the influence of temperature and salinity on nanoparticle stability and reported several historical cases of applying nanoparticle dispersions with acid for asphaltene remediation [8]. Influence of those factors on the organic compounds grafted on the inorganic templates can be more complicated. Apropos of amphiphilicity, different surfactants have different optimal salinities and pH values, at which interfacial tension will reach its minimum value. The optimal salinity and pH value are normally measured by an IFT screening test [85]. Low IFT value will increase oil recovery ratio dramatically[86,87]. In addition to salinity and pH value, the relationship between temperature and interfacial tension has also been studied for molecular surfactant systems [88]. It has been reported that due to effects of chemical stability and electric interaction, high salinity and high temperature will degrade or destabilize molecular surfactant, which is also expected to happen for the surface modifications on the nanomaterials [89]. A thorough surface chemistry compatibility check is suggested.

1.4.4. Surface Modification of Nanomaterial

Surface modification can affect nanoflooding at two different aspects. First, surface functional groups control material dispersion and aggregation through particle polar or non-polar interactions. These particle interactions will affect material stability dispersibility during application. Then, particle surface chemistry determines factors like, particle retention, wettability alteration, and ability to emulsify and stabilize emulsions or foams, which will affect flooding performance directly. The material physical properties,

such as density and magnetic response, are dictated by pristine material properties; however, with proper surface modification, material surface properties can be controlled. Well-designed surface modifications can change particle hydrophobicity, and thus alleviate particle retention on the rock surface. A lower particle retention is desired, as particle retention is one of the direct causes for formation damage. Rodriguez *et al.* reported their observations on particle retention of polyethylene glycol (PEG)-coated silica particles. They observed that surface coating naturalizes surface charge on silica particles. As a result, their system has less particle retention compared to other peer research [68]. Surface charge modification and particle retention are also explained theoretically by Monfared *et al.* They studied adsorption of silica nanoparticles on calcite, interpreted obtained data with DLVO theory, and found adsorption follows a second-order model [90].

Janus particle modification is a special particle surface modification which is very promising to be applied in nanoflooding. In a typical procedure, different functional groups or hydrophobic and hydrophilic polymers will be grafted on the two sides of particles to achieve smaller interfacial tension. Also, nanoparticles with heterogeneous and amphiphilic surface modification are more stable at interface than those with homogeneous surfaces [91]. Efforts have been made to review the synthesis of Janus particle surfactants [28,92], such as the earlier paper reported by Takahara *et al.*[93] on Janus silica nanoparticles. Particles were synthesized at the water/oil interface by introducing silane in oil phase. The as-synthesized product is proved to be surface-active by the grafting of gold nanoparticles on the hydroxyl group of silica nanoparticles, and surface tension was

quantified with a pendant drop measurement. By applying Au/Fe_3O_4 at the hexane-water interface, Glaser *et al.*[24] observed a sharp decrease of interfacial tension, and interfacial tension observed on Janus particle systems was observed to be lower than that of non-Janus particles. The same conclusion can be drawn from reports from other researches; for instance, Fernandez-Rodriguez's work on homogeneous and Janus gold nanoparticles [94]. They reported that surface functionalized Janus particles exhibited better surface activity than homogeneously functionalized gold particles in all testing conditions. As mentioned earlier, reduced interfacial tension can play an important role in displacement of formation residue oil. Moreover, by proper surface modification, emulsification can also be reversibly controlled [69]. Such precise control of emulsification and de-emulsification enables delivery of reagents to desired specific targets in the underground formation.

1.4.5. Material External Field Response

Wisely utilizing intrinsic material properties can facilitate oil recovery procedure. Such intrinsic property could be electrical [95], magnetic [96, 97, 98], rheological [99, 100] and thermal [100] properties. Yahya *et al.* [101] presented their work on cobalt ferrite nanoparticles with electromagnetic waves, which is a very promising method for heavy oil recovery. The magnetic particle would be self-heated under high frequency electromagnetic waves. Then nanoparticles conduct the heat to the surrounded crude oil, reducing the viscosity of crude oil and increasing oil recovery. Ferrofluid is a suspension of paramagnetic materials. Applying ferrofluid for enhanced oil recovery has also been proposed and demonstrated in laboratory[102].

CHAPTER II

INORGANIC TEMPLATE SELECTION FOR SURFACE ACTIVE NANOPLATE

2.1. Material Selection

Choosing a proper inorganic template is a vital step to synthesis functional nanoplatelets, because particle size, particle geometry and surface chemical groups varies between different minerals. During the initial step of my research, I investigated different inorganic minerals and tried to find the best candidate for the surface modification step. I tested different prospective inorganic materials for surface modifications during initial step, which includes, Kaolinite, Graphene Quantum Dots (GQD), Laponite, Halloysite and Montmorillonite. These materials are analyzed and evaluated for later asymmetric modification and Janus surfactant synthesis. Selection is made based on material morphology, surface functional groups and surface chemistry versatility.

2.1.1. Kaolinite

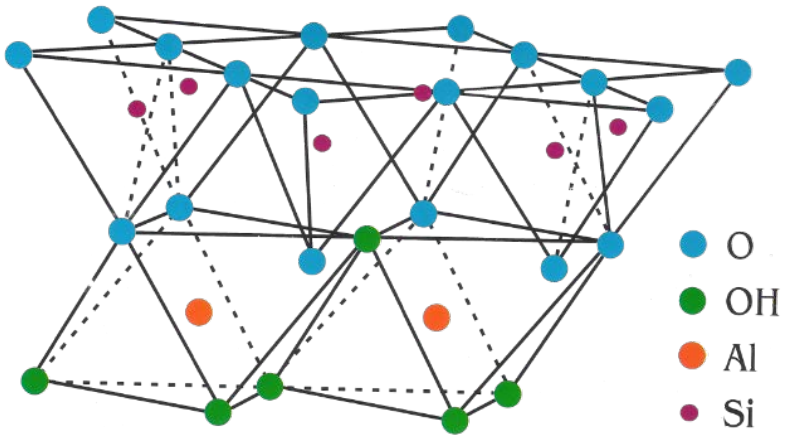

Figure 8. Crystal Structure of Kaolinite

Kaolinite is a common clay and has been used as an important raw material in different industry sectors. The silicate mineral has a sheet of tetrahedral Silica units linked with another layer of octahedral Alumina units through oxygen atoms between two layers (Figure 8). The structure of Kaolinite endows its asymmetry intrinsically. The –OH group on top and bottom surfaces greatly simplified modification process of Kaolinite mineral. The other reason we choose Kaolinite as our primary candidate for further modification is the low cost of raw material. Price of washed raw kaolinite is about $120 per metric ton. Last but not least, because Kaolinite has a long history of application in different industries, surface modification of Kaolinite is thoroughly studied. Various surface modification strategies have been reported by different research groups. Gardolinsky [103] reported their work on Kaolinite intercalation with DMSO and different diols by changing intercalation molecules. After intercalation, they grafted diol in the inner surfaces (Figure 9). Though interaction between diol and Kaolin is coordinate bond, this work proved the possibility to use polar solvent to intercalate layered kaolinite, then conduct surface modification. Kuroda [104] simplified kaolinite intercalation by using iron liquid to exfoliate kaolinite in one-step. Interestingly, the exfoliated kaolinite tends to scroll in to rolls (Figure 10). Other researchers, including Hirsemann has reported directly graft kaolinite with ethylene glycol [105-107].

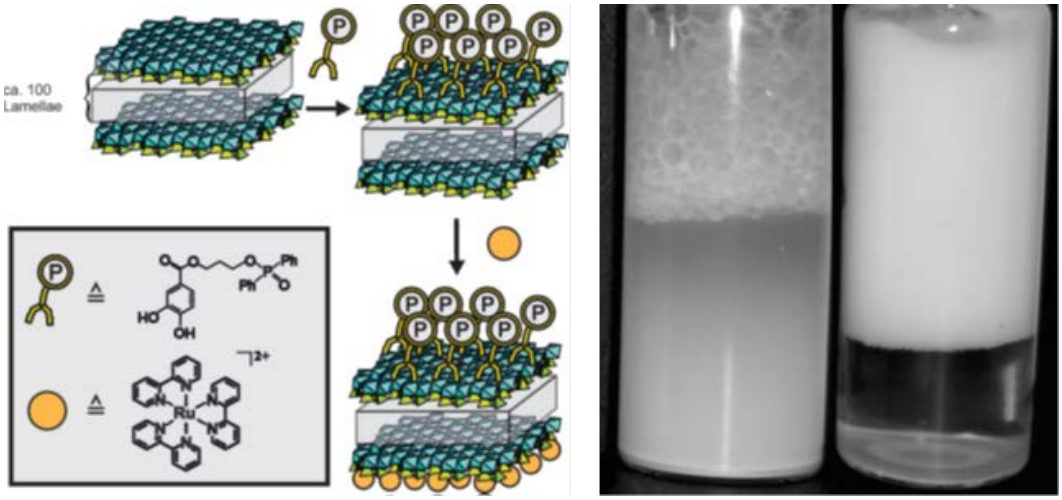

Figure 9. Janus platelets synthesized by ion exchange and glycol covalent grafting (Left), Emulsion formed with the as-synthesized Janus platelets (Right) (Reprinted with permission from[105]).

To verify the possibility to use kaolinite as a template to synthesis surface active nanoplatelets, a surface modification trial was carried out. Kaolin sample was purchased from Arcros (Kaolin, Pure). Sample then was processed with EDTA to remove absorbed Calcium and Magnesium ions. To remove Ferric oxides, kaolinite was stirred with citrate−bicarbonate, then with dithionite. This iron removal process is known as DCO method [108]. Later samples were washed with excessive DI water, free-dried then stocked for modifications. SEM pictures were taken for the washed samples, as shown in Figure 11 and Figure 12. We also attempted to synthesized small size kaolinite platelets with Na_2SiO_3 and $Al_2(SO_4)_3$ through hydrothermal method, however, XRD measurement does not show strong Kaolinite peak (Figure 13).

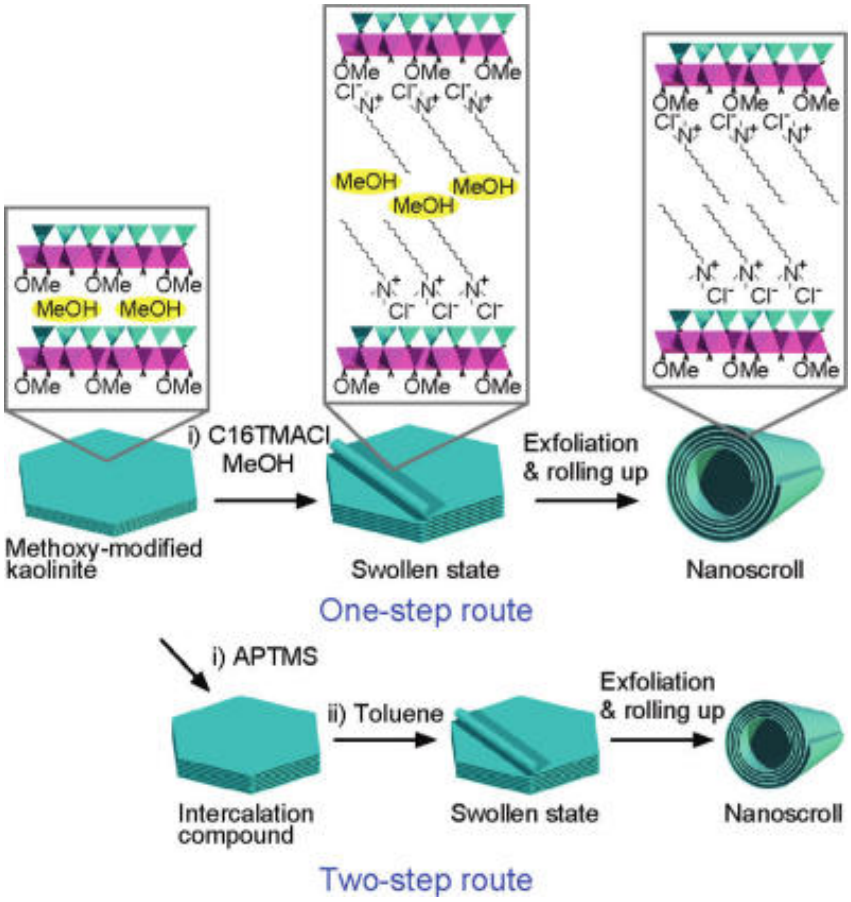

Figure 10. Intercalation and modification method proposed by Kuroda et. al.[104]

Atom transfer radical polymerization (ATRP) of kaolinite has been reported by other researchers before [109]. The ATRP is performed in an oil in water emulsion to ensure simultaneous modifications on both side of platelets. Hydrophilic surface modification is carried out by N-isopropylacrylamide (NIPAM) polymerization, using Copper(II) bromide as catalyst and PMDTA as ligand, α-bromoisobutyric acid as reaction initiator. Hexane and water emulsions are prepared to compare the emulsification behavior between pristine kaolinite and Janus kaolinite.

From the characterization of kaolinite, we think the Kaolin clay material is a good candidate for asymmetric modifications. There are several reasons: Firstly, Kaolinite surfaces has intrinsic asymmetry. Secondly, surface μ-Hydroxyl group has different possibility to be modified with diol, silane or another functional group. Lastly, surface ATRP is proven on the kaolinite system. The only potential challenge with kaolinite is the axial size (material thickness). To be applied in enhanced oil recovery, surface active particles should be able to pass throat at downhole. Particle size should be controlled at a relatively low range. From SEM observation, the average size of this kaolinite sample is 0.4 μm. To further reduce particle size, two potential solutions have been considered. First, mechanical grinding should be a feasible way to reduce kaolinite surface size. Another alternative will be synthesized kaolinite with bottom up method.

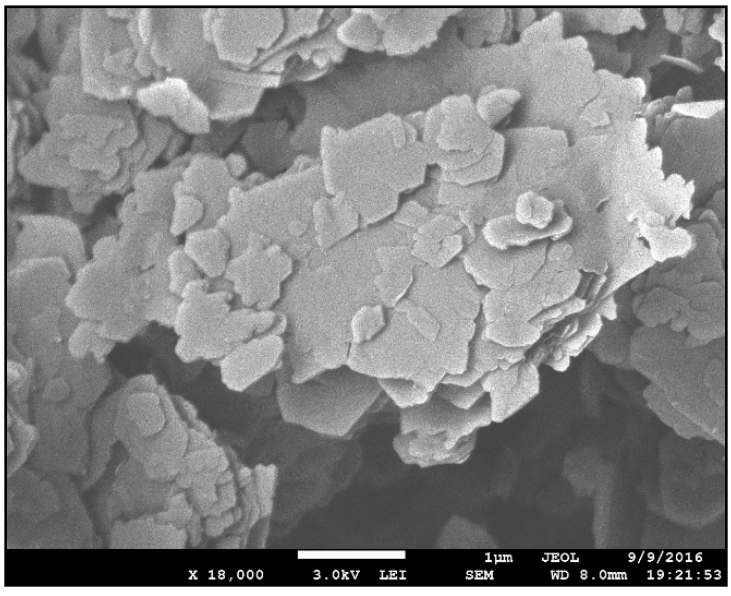

Figure 11. SEM picture of Kaolinite (Washed), High Magnification

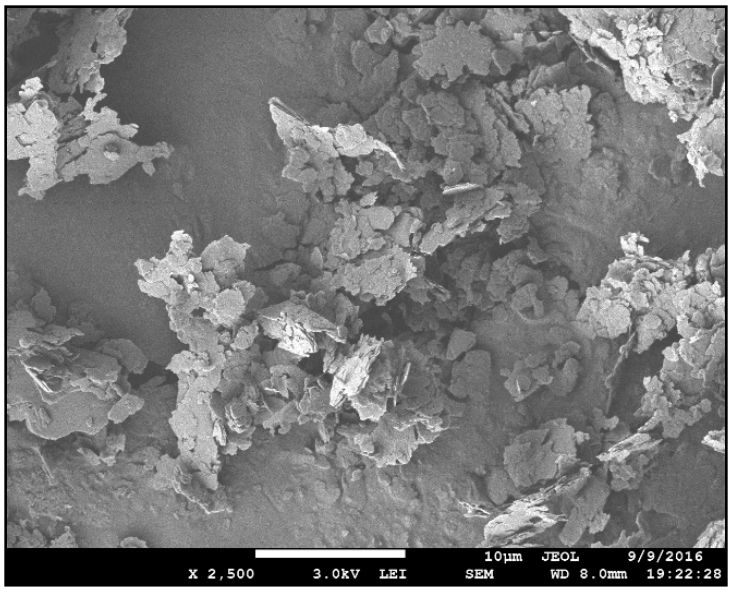

Figure 12. SEM picture of Kaolinite (Washed), Low Magnification

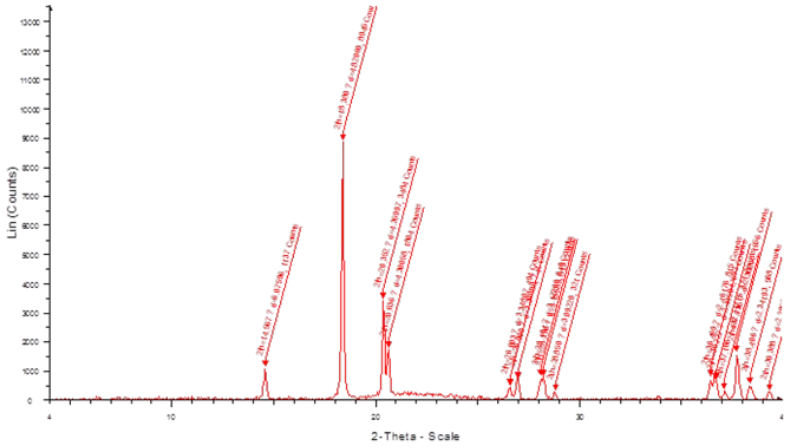

Figure 13. XRD data for synthesized Kaolinite sample, characteristic peak of Kaolinite at 13° and 25° were not observed.

2.1.2. Halloysite

Halloysite is a natural aluminosilicate with similar crystal structure as kaolinite. The only difference between Halloysite and Kaolinite is that Halloysite has nanotube

structure. The curling of Halloysite is because of the misfit between Al octahedral and Si tetrahedral [110]. Chemically, the outer surface of the Halloysite nanotubes is Si tetrahedral and has properties similar to SiO_2; while the inner cylinder core is related to Al_2O_3. Surface modifications of Halloysite has also been reported. The outer Silica surface can be easily modified with Silane [111], and modification on inner Alumina side has also been reported[112]. Halloysite has been used for stabilizing some hydrophobic compound and proved to be a successful drug delivery vessel [113]. It has been reported that Halloysite can be extended into nanoplates with specific phosphonic acid modifications [114,115]. Additionally, Halloysite nanoplates possess an asymmetrical crystal structure with the alumina on one side and the silica on the other side. This intrinsic asymmetry makes selective surface modification possible and facilitates the fabrication of Janus structure. Phosphonic acids, a type of common surface modifier [116,117], can specifically react with the alumina side of the Halloysite clay, but not the silica side [112,118,119]. This selective surface modification can change the wetting property on the alumina side and further mask the alumina side of the nanoplate to protect it from later chemical modification, simplifying the modification of silica side.

Halloysite sample is purchased from Sigma-Aldrich (Halloysite, Nanoclay), then washed with DIW, freeze-dried and stocked for future modification. Several trials have been made to unfold the natural Halloysite into kaolinite form.

With the exactly chemical structure as Kaolinite, Halloysite will be a good alternative route for asymmetric modification. Benefit from its scrolling morphology, we think it will be easier to modify Kaolinite asymmetrically.

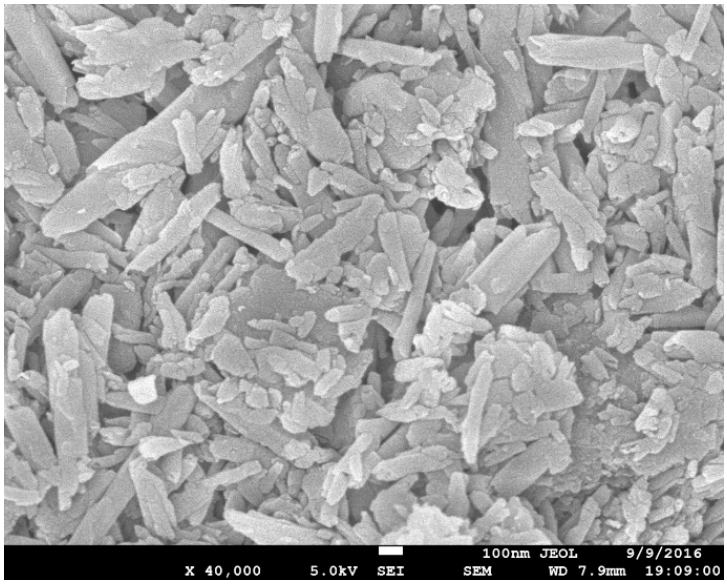

Figure 14. SEM picture of Halloysite (Washed), Low Magnification

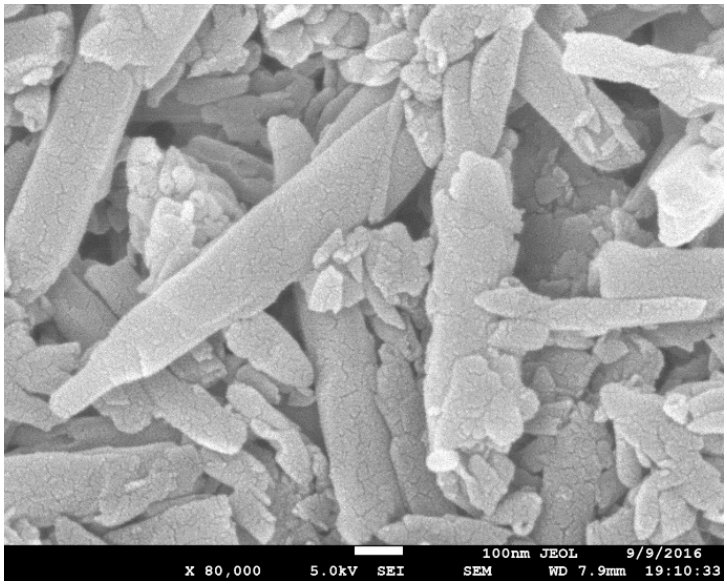

Figure 15. SEM picture of Halloysite (Washed), High Magnification

2.1.3. Graphene Quantum Dots (GQD)

Although application of microscale graphene sheets for emulsification purpose has attracted much attention recently, nanoscale graphene platelets, such as graphene quantum

dots (GQDs), have been rarely explored in interface science. Our group synthesized amphiphilic luminescent graphene quantum dots [120].Several batches of hydrophilic p-GQDs had also been prepared according to method in previous work [121]. Comparing to Kaolin clay material, the disadvantage of GQD is lack of surface asymmetry, although the size of GQD is smaller than Kaolin group clays.

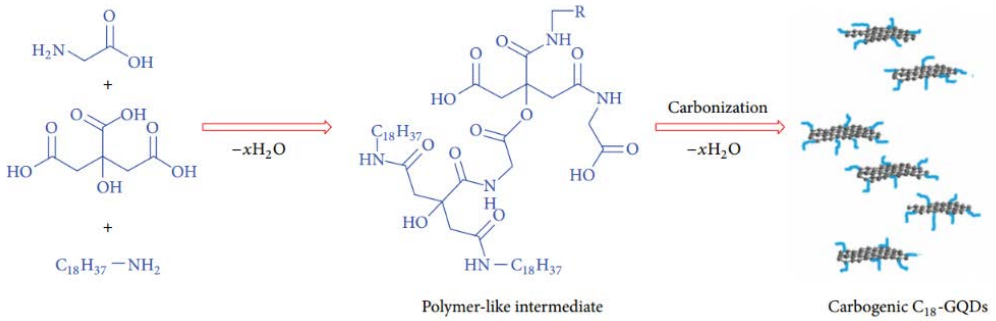

Figure 16. Synthesis Schematic of Graphene Quantum Dots[120]

2.1.4. Montmorillonite

Like Kaolinite, Montmorillonite is another common clay with wide applications. The structure of Montmorillonite is only slightly different from Kaolinite. Instead of the tetrahedral-octahedral structure of kaolinite, a Montmorillonite crystal unit has a tetrahedral-octahedral- tetrahedral structure. Exchangeable cations and structure water are fixed between different layers. Owing to its high ion exchange capacity, Montmorillonite is a common heavy metal absorbent. Different research groups have tried different methods to modify montmorillonite surfaces. Sun used quaternary ammonium surfactant to modify Na-montmorillonite in alkane solvents, the obtained montmorillonite has a better dispersibility in alkane solvents [122]. Montmorillonite K10 sample is purchased from Fisher Chemical. Sample is washed with Deionized water and freeze-dried for stock. SEM

image is capture to characterize montmorillonite morphology. Platelets size is between 1 µm to 10 µm. The particle size is too large to pass through pore throat. Comparing to Kaolin group clay material, montmorillonite lack of surface asymmetry.

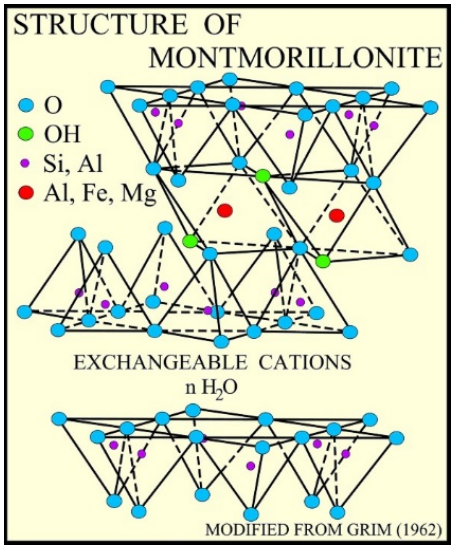

Figure 17. Montmorillonite structure. (Reprinted with permission from U. S. Geological Survey Open-File Report 01-041)

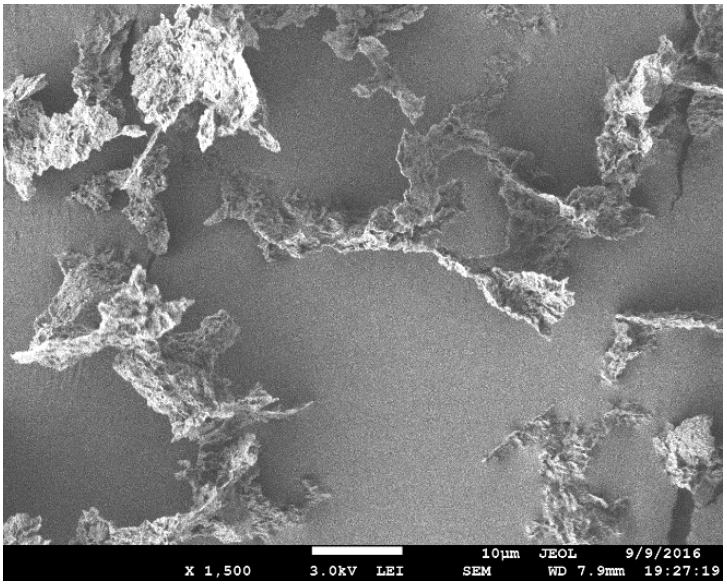

Figure 18. SEM picture of Montmorillonite (Washed), Low Magnification

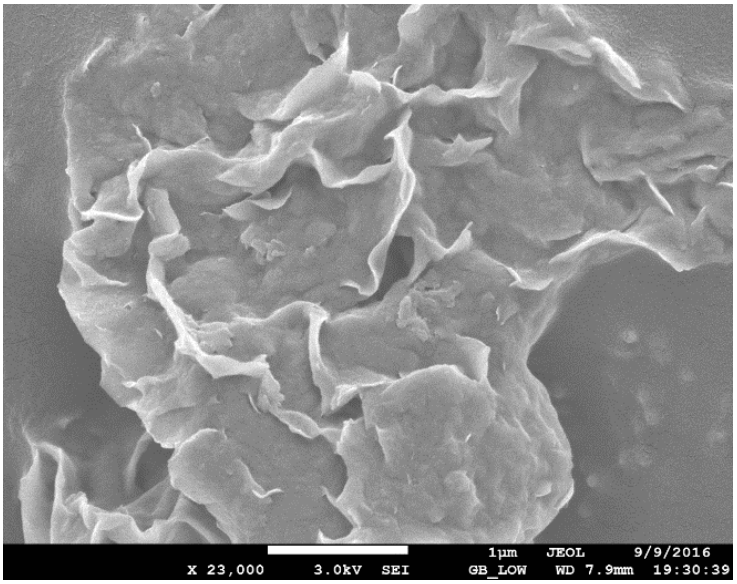

Figure 19. SEM picture of Montmorillonite (Washed), High Magnification

2.1.5. Laponite

Laponite is a common industrial additive for rheology modification, more importantly, because of its uniform size distribution, Laponite also serves as a model system to study nanoplatelets phase behavior [123]. Different researchers have modified surfaces of laponite nanoplatelets. However, because of surface charge difference, those platelets tend to self-aggregate, which makes surface modification unsuccessful [123]. Our Laponite RDS sample is acquired from BYK additives Co. Figure 21 shows strong aggregation of Laponite nanoparticles because of different surface charge. The strong surface charge is causing problem for surface modification.

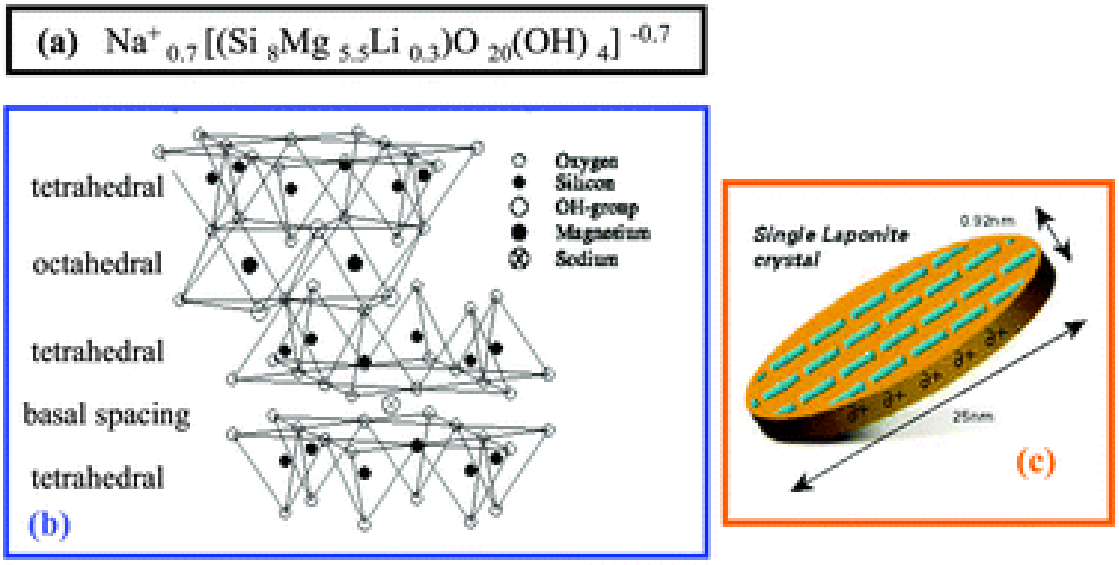

Figure 20. (a) Empirical formula of Laponite. (b) Idealised structural formula of Laponite drawn in perspective. (c) Single Laponite platelet[123].

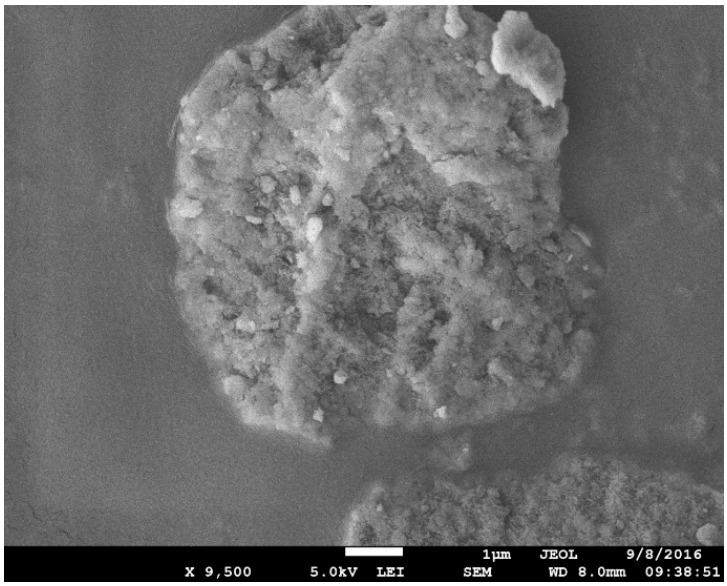

Figure 21. Laponite RDS sample under 9,500 magnification.

2.2. Summary of Chapter

The crystal structures of Kaolinite, Halloysite, Graphene Quantum Dots, Montmorillonite and Laponite RDS have been studied and compared. Among these

substrates Kaolinite group materials Kaolinite and Halloysite have asymmetrical structure, and the surface hydroxyl group also creates convenience for later modification. However, unprocessed Kaolinite is stacked up by many layers of crystal unit. To obtain single layered structure, exfoliation method and bottom-up synthesis have been explored. A simpler method to obtain thin layer of Kaolin crystal would be unscrolling of Halloysite.

CHAPTER III

NATURAL HALLOYSITES-BASED JANUS PLATELET SURFACTANTS: FROM PICKERING EMULSIFICATION TO ENHANCED OIL RECOVERY [†]

3.1. Technical Background

Despite the development of renewable energy sources, fossil fuel will remain as the dominant energy resource in the global energy supply for decades. According to U.S. Energy Information Administration's (EIA) projection, fossil fuels will supply 75 quadrillion (10^{15}) BTU of energy by 2050 to meet the world energy demand [124]. On the production side, production from aging wells will be reduced from current levels. Unless certain stimulation measures are taken, production on an aged well will be less economically viable for oil recovery. Enhanced oil recovery (EOR) is a common well stimulation method to increase productivity of oil wells. Conventional EOR is carried out with molecular surfactants; however, harsh formation conditions, such as high temperature or high salinity, can decrease the efficiency of molecular surfactants or polymer systems. Particle-stabilized emulsion, also known as Pickering Emulsion, might provide an alternative solution [125].

Pickering emulsions and foams are immiscible mixtures stabilized with solid particles instead of molecular surfactants. Compared to emulsions stabilized by conventional molecular surfactants, Pickering emulsions are more stable due to their

[†] Part of the data reported in this chapter is reprinted from Zhang, L., Lei, Q., Luo, J. et al. Natural Halloysites-Based Janus Platelet Surfactants for the Formation of Pickering Emulsion and Enhanced Oil Recovery. Published 2019, Scientific Reports.

resistance to coalescence (a process in which emulsion droplets merge together) and Oswald ripening (a process in which content in emulsion droplets diffuse through medium and eventually merge together)[126-128], which makes it perfect candidate for industrial application in foods emulsification[129,130], mining[131,132], drug delivery[133] and cosmetics [134]. A variety of nanoparticles with different morphologies have been used to stabilize Pickering emulsions, such as zero-dimensional nanoparticles,[82] one-dimensional nanowires[135], and one-dimensional nanotubes[136]. Among different particle morphologies (nanospheres, nanorods and nanoplates), the idea of applying two-dimensional disks or platelets to stabilize emulsion attracts more attention[137-139]. There are several merits for doing so: firstly, the two-dimensional sheets can provide greater surface coverage than other configurations, which can prevent the emulsified phase from diffusing to the continuous phase. Also, the large surface coverage area significantly increases the magnitude of energy required to remove platelets from the interface. Lastly, the two-dimensional configuration has higher efficiency in terms of material utilization compared to spherical or cylindrical geometries[61]. These merits contribute to the enhanced stability of Pickering emulsion, low coalescence and ripening rate and high material efficiency.

Emulsion stability varies directly with interfacial energy, a characteristic which has been well analyzed in other peer works[140,141]. Interfacial energy, is related not only to particle geometry, but is also controlled by surface wetting property. To minimize interfacial tension, asymmetric surface modification may be applied to satisfy different wetting preferences on each sides of the platelet to different fluids. Such amphiphilic structure of a nanoplate is also known as a Janus platelet, which has been previously

reported by our group[63,142]. Although the amphiphilic platelets have the potential to be used to stabilize emulsion, the current synthesis methods for such platelets are not efficient for mass production. Mask-and-modify, as an example, is a very common strategy for Janus platelet synthesis[143]. Masking can be achieved on either emulsion interfaces[109] or solid substrates[144], but regardless of procedure, reaction can be carried out only at the interface of emulsion droplets, rendering these methods tedious and not suitable for industrial applications. Another method, Modify-then-exfoliate, is more efficient than the mask-and-modify method as it allows bulk reactions rather that limiting reactions to a two-dimensional interface. Although the synthesis of Janus platelets by the modify-then-exfoliate method is more efficient, the yield of Janus platelets is still limited, and less desired Gemini platelets will be generated[63]. Careful choice of inorganic template will avoid the formation of Gemini platelets[145]. The yield of final product, however, is still limited by the exfoliation or cleaving process. Last but not least, Some researchers[105] realized the simplicity of employing asymmetrical substrates, such as kaolinite, for Janus particle synthesis. Covalent grafting on both sides was not achieved, however, which may limit the salinity tolerance of the final surfactant product.

In this thesis, I am presenting a two-step versatile method to synthesize a new kind of surface-active nanoplate to stabilize Pickering emulsions. The nanoplates are obtained by grafting phenyl phosphonic acid on the alumina side of Halloysite as the nanoscroll extends after its alumina side reacting with phenyl phosphonic acid. Yet the phosphonic acid modification does not merely flatten the Halloysite nanoscrolls, it also serves as the hydrophobic surface modification and a masking layer to protect the alumina from later

reactions. A surface-initiated ATRP is furtherly carried out on the silica side to render the surface hydrophilic. The product is characterized with different methods to confirm the success of asymmetrical modifications. The interface of Pickering emulsion stabilized by such nanoplate surfactant is studied in detail. Furthermore, an application demonstration is conducted with microfluidic chip to explore the possibilities to apply Janus platelet surfactant for enhanced oil recovery.

3.2. Synthesis Procedure

3.2.1. Preparation of Synthesis

Halloysite nanoclay (Sigma-Aldrich™), phenyl phosphonic acid (PPA, 98%, Sigma-Aldrich™), 3-aminopropyl triethoxysilane (APTES, 99%, ACROS Organics™), triethylamine (TEA, 99%, ACROS Organics™), bromo-isobutyryl bromide (BiBB, 98%, Sigma-Aldrich™), Dimethylamino ethyl methacrylate (DMAEMA, 98%, Sigma-Aldrich™), ethyl α-bromoisobutyrate (ETBriB, 98%, Sigma-Aldrich™), copper monochloride (CuCl, 97%, Sigma-Aldrich™), toluene (anhydrous, 99.8%, Sigma-Aldrich™), Toluene (Certified ACS, Fisher Sci.™), dichloromethane (DCM, anhydrous, ≥99.8%, Sigma-Aldrich™), isopropanol (Certified ACS, Macron Fine Chemicals™), Sudan IV(Fisher Chemical), styrene (≥99.5%, Sigma-Aldrich™), azobisisobutyronitrile (AIBN, Sigma-Aldrich™), octyl triethoxysilane (≥97.5%, Sigma-Aldrich™) were used without further purification.

3.2.2. First Step: Synthesis of Single-Side Modified Halloysite Nanoplatelets

For better illustration purpose, a scheme of synthesis procedures are summarized in Figure 22. In a typical experiment, 25 grams of PPA and 25 grams of halloysite were

suspended in 500 mL of deionized water (DI water) in a one-liter flask and then immersed into 70 °C oil bath with gentle stirring for 3 days. After that, the halloysite with a modified alumina side was washed three times with DI water and freeze-dried. The unscrolled halloysite with PPA modifications on one side was stocked for further reaction. The grafted PPA on the alumina side serves as a hydrophobic modification and protects the alumina side from further reactions during subsequent hydrophilic modification steps.

3.2.3. Step Two: Synthesis of Janus Nanoplates

Surface-initiated atomic transfer radical polymerization (si-ATRP) method is employed to modify the silica side of the clay platelet. To immobilize surface initiator on the silica side of Halloysite clay sheet, 0.5 g PPA-modified Halloysite was initially suspended in 40 ml of anhydrous toluene. Then high-power probe sonication was applied for 5 to 15 minutes to ensure a good dispersion of nanoplates in solvent and to reduce aggregation, so that material surface can be evenly modified. After sonication, APTES (10 ml) was injected into the flask with a dry syringe for salinization, with oxygen free atmosphere in the flask, normally through Argon or Nitrogen purge. The reaction was conditioned at 70 °C with constant magnetic stirring. After salinization was complete, the product was centrifuged and washed three times with toluene to remove residual free silane. In the second part of the reaction, bromide initiator grafting was conducted. In a typical experiment, 0.5 to 1.5 grams of Halloysite platelets with amino group terminals on the silica side were re-dispersed in anhydrous dichloromethane (DCM). Then, bromo-isobutyryl bromide (BiBB) was introduced to react with amino groups on the silica side. At the same time, triethylamine (TEA) was added to neutralize the by-product. Quantity

of TEA depends on Halloysite and BiBB. This step is conducted under room temperature with stirring for 3 to 8 hours. After platelets with surface initiators were prepared, ATRP was performed in isopropanol. In our surface-initiated ATRP reaction, we chose DMAEMA as monomer, EtBriB as free initiator, PMDETA as ligand, and CuCl as catalyst. The final product was washed and centrifuged with isopropanol three times, with DMF three times, and then with DI water once to remove any free polymers or monomers. The final product was freeze-dried and stocked for later application and characterizations.

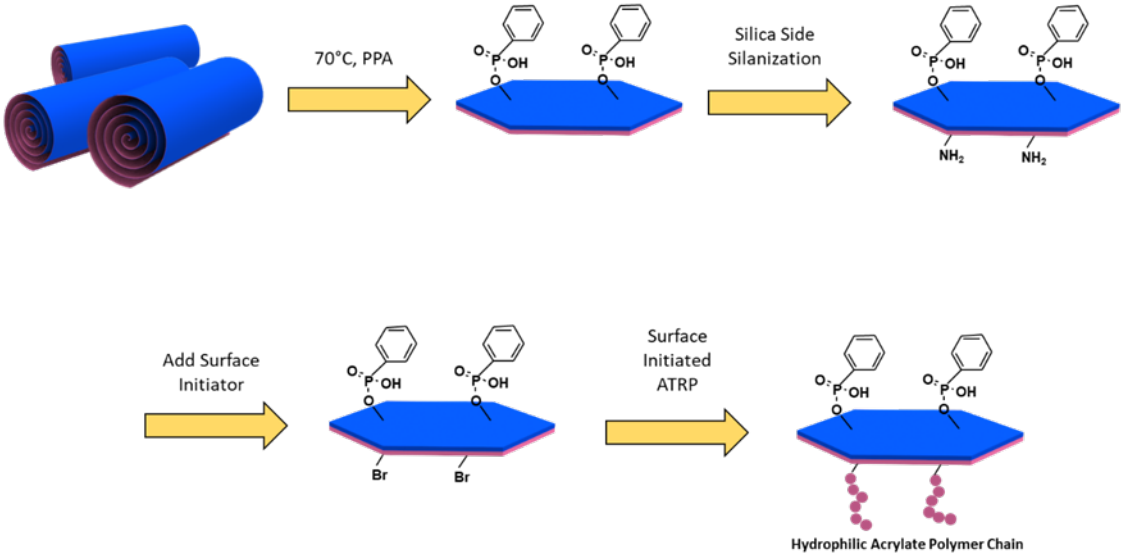

Figure 22. Synthesis flowchart of Janus nanoplate surfactants. Blue side represents the octahedral alumina side of halloysite and unscrolled halloysite, and magenta represents the tetrahedral silica side of halloysite and unscrolled halloysite. First, halloysite scroll is extended and grafted by PPA on the alumina side, followed with silanization on the silica side and surface-initiated ATRP reaction. The final platelet surfactant is rendered with distinct hydrophilic polymer and hydrophobic phenyl group on each side, respectively.

3.3. Characterizations of the Janus Nanoplates

3.3.1. Chemical Characterization Methods

The sample prepared using the above methods was characterized by transmission electron microscopy (TEM, JEOL JEM-2010) and scanning electron microscopy (SEM, JEOL JSM-7500F) under different magnifications and voltages to observe the morphology of raw Halloysite precursors, unscrolled Halloysite sheets, Janus nanoplates, and the polystyrene sphere surface stabilized by Janus nanoplates. Fourier-transform infrared spectroscopy (FT-IR, Thermo Nicolet 380 FT-IR spectrometer) and magic-angle spinning solid-state NMR (MAS ssNMR, Bruker Avance-400 spectrometer) were used to characterize the success of surface modifications. Interfacial tension was measured with a bench-top pendant-drop tensionmeter and a python algorithm[146]. In a typical measurement, about 10 μL platelet surfactant suspension was dispensed with a micro syringe and high gauge needle into an optical cuvette, which was filled with an oil-phase solution, and image of droplet morphology was captured by a webcam and processed with a computer. With the python algorithm, computer calculates IFT according to the fitting of droplet curvature.

Contact angles were measured with a SupereEye USB microscope (Version 7.0) mounted on an optical table to demonstrate wettability alteration induced by Janus nanoplate.

3.3.2. Microfluidic Flooding Simulation for EOR

An on-chip flooding experiment was performed with a glass microfluidics model. The microfluidics model (Design 1 Solution), was manufactured with a pockets pattern

design, two inlets, and one outlet. Each pocket was configured as a 300 μm × 300 μm square with a 150 μm × 20 μm groove in the middle. Sudan IV-dyed dodecane was injected as an oil phase to saturate the microfluid chip. The chip was then left aside to react with the oil for a week. DI water was then injected into the chip reservoir with a syringe pump to simulate water flooding. After the chip reached a stable condition, which means no more oil can be recovered solely by water flooding, the flooding phase was replaced with the 0.25 weight % platelet surfactant suspension. Images captured before and after platelet suspension injections were processed with ImageJ to calculate oil recovery ratio.

3.3.3. Chemical Characterization Result and Discussion

To confirm the success of surface modification, FT-IR and ssNMR are used to characterize different samples. The ATR FT-IR spectra (Figure 23) are obtained with a Thermo Nicolet 380 FT-IR spectrometer. Comparing PPA-Halloysite spectrum to Halloysite spectrum, a strong peak appears at 1438 cm^{-1}, which is attributed to the stretches of benzene ring. The benzene peak indicates the successful grafting of PPA onto the Halloysite sample. Spectrum of PPA-Halloysite-PDMAEMA is also collected with similar procedure. Comparing it with the PPA-Halloysite and Halloysite spectra, the new peak of PPA-Halloysite-PDMAEMA at 1728 cm^{-1} is produced by the C=O stretching of DMAEMA polymer. These IR spectra proves the success of the surface modifications on the clay platelets.

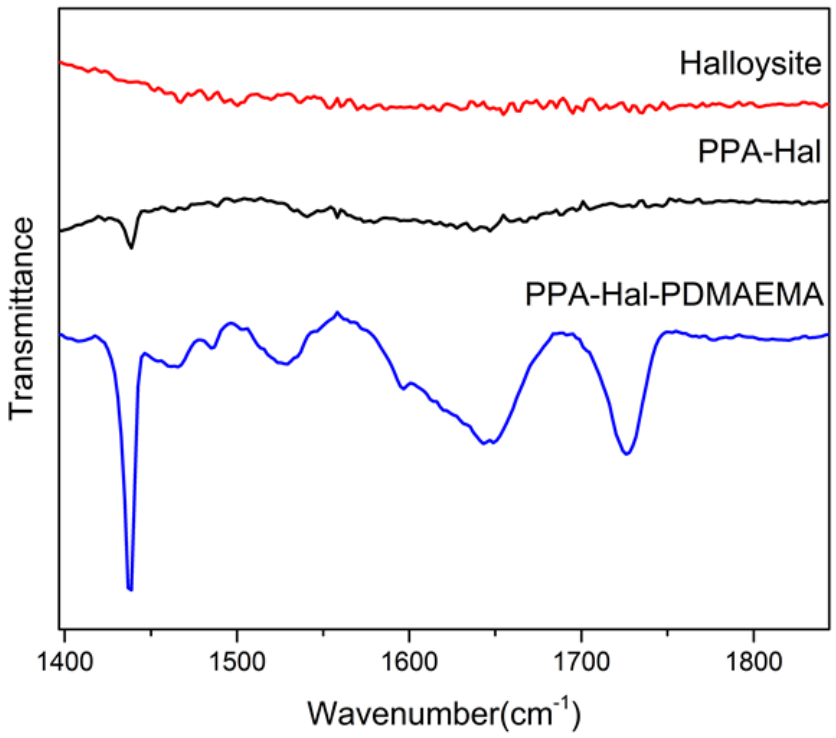

Figure 23. FT-IR spectra of pristine Halloysite (red), PPA-modified Halloysite (PPA-Halloysite, black), and Janus nanoplate, the asymmetrically modified Halloysite (PPA-Halloysite-PDMAEMA, blue). After alumina side modification, benzyl characteristic peak (1438cm^{-1}, ring deformation) is observed on the PPA-Halloysite spectrum after alumina-side PPA modification. PDMAEMA characteristic peak (1728cm^{-1}, carbonyl stretching) is observed after silica-side ATRP modification.

To further confirm asymmetric modifications on platelets and chemical environmental changes of Al and Si elements after modifications, ssNMR spectra of pristine and modified clay are obtained with a Bruker Avance-400 spectrometer (400 MHz for 1H nuclei) with a standard 7-mm MAS probe at different spinning rates, as shown in Figure 24. The -10ppm peak in the pristine Halloysite corresponds to the chemical environment of Al on the alumina side before modification. After PPA surface

modification, another peak at 28 ppm appears, which is attributed to the PPA-modified Al atoms. A couple of satellite peaks are also observed at the 21 ppm and 46 ppm positions.

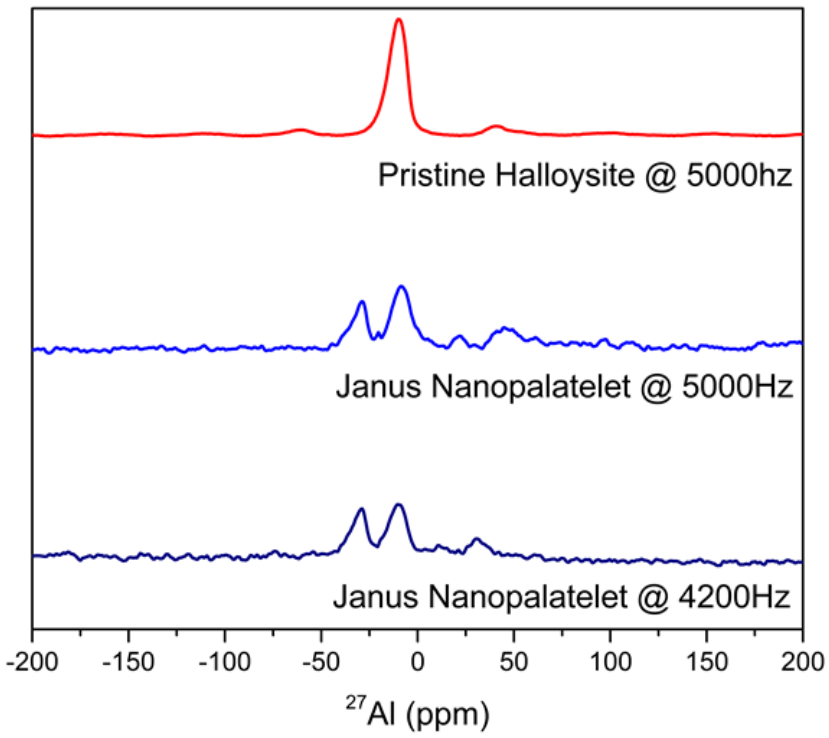

Figure 24. ^{27}Al MAS ssNMR spectra of pristine Halloysite (blue), Janus nanoplate (PPA-Halloysite-PDMAEMA, red) @ 5 kHz. Janus nanoplate (PPA-Halloysite-PDMAEMA, red) @ 4.2 kHz;

To confirm those satellite peaks, the frequency is changed to 4.2 kHz, we observed shifts of peak positions to 11ppm and 31ppm, indicating the presence of satellite speaks. The 28-ppm peak attributed to PPA remains the same, suggesting that the PPA has selectively reacted with the alumina side. However, no chemical shift was observed in the ^{29}Si MAS ssNMR spectra (Figure 25), which indicates before and after PPA modification, Si chemical environment does not change. Combining the ^{27}Al ssNMR data, we draw the

conclusion that the PPA will only graft on the alumina side and leaves silica side intact, which makes surface modification totally asymmetric.

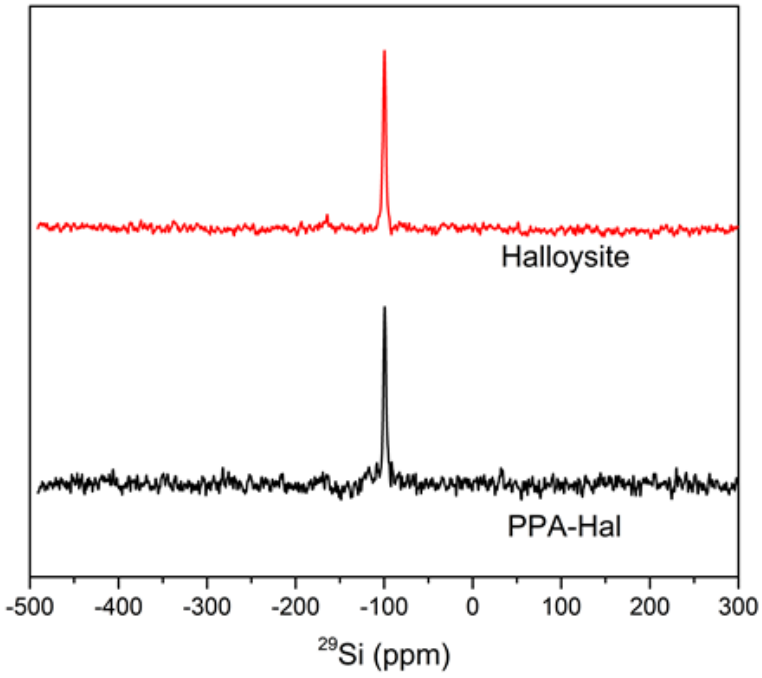

Figure 25. Solid-state nuclear magnetic resonance spectrums. ^{29}Si MAS NMR spectrum @ 5KHz of pristine Halloysite (Top), shows a strong peak at 99.34 ppm. After alumina side PPA modification, ^{29}Si MAS NMR spectrum is measured again (Bottom). No significant shift has been observed, which confirms that PPA will not react with Si during the Al side hydrophobic modification procedure.

We made an effort to measure the ^{29}Si MAS ssNMR spectrum after ATRP reaction. However, due to the strong shielding effect caused by Cu^{2+}, which was introduced during the ATRP reaction as a catalyst, no ^{29}Si signal can be detected. A ^{13}C MAS ssNMR spectrum was measured for the PPA-Halloysite-PDMAEMA sample. The peak at 398.00 ppm is produced by the carbonyl group from PDMAEMA; the peak at 131.66 ppm is

attributed to phenyl group from PPA, which again, suggests the successful surface modifications on the alumina side and silica side (Figure 26).

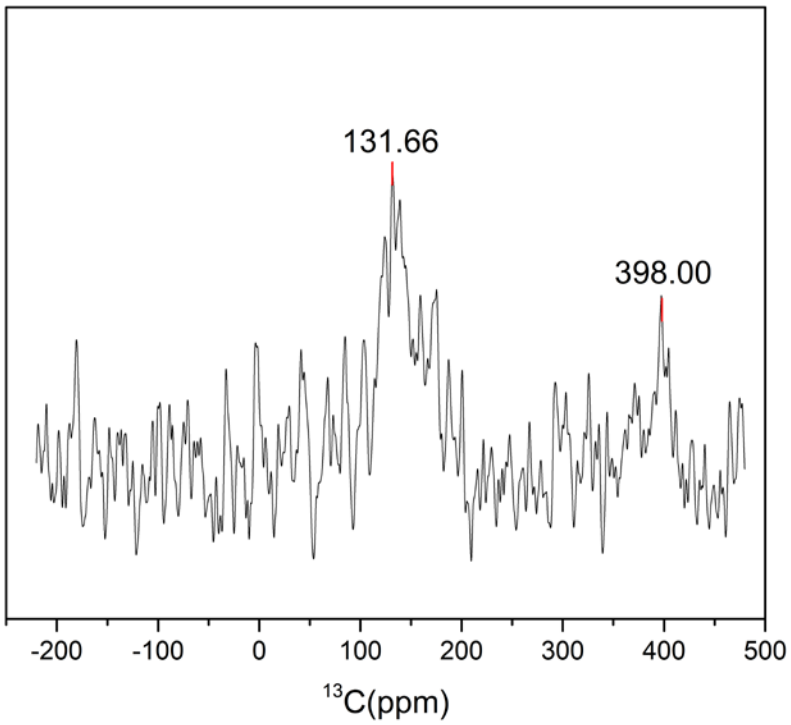

Figure 26. Solid state ^{13}C NMR spectrum of asymmetrically modified nanoplate surfactant, it confirms the successful amphiphilic modifications on both sides of the nanoplates.

The TEM (Figure 27a) and SEM (Figure 28a) images of pristine Halloysite present the typical morphology of the aluminosilicate clay material, which is a hollow tubular scroll with a multiple-layer wall. Because the nanoclay is processed from natural clay material directly, the diameter, length, and aspect ratio of Halloysite raw material are widely distributed. The main morphology of pre-processed Halloysite, however, remains as hollow nanotubes. After reacting with PPA, the hydroxyl group from the PPA forms a

covalent bond with the hydroxyl group on the alumina side of Halloysite and unscrolls the multiple-layer wall nanotube into a nanoplate. The morphology changes from tube to platelet due to the hindering effect caused by the inserted benzene group between layers and the weakened hydrogen bond.[112,114,115,118] The morphology change is manifested by comparing the pristine Halloysite electron microscopic images with the modified particle images (Figure 27b and Figure 28b).

After the silica-side salinization and surface ATRP reactions, the nanoplates morphology remains the same (Figure 27c and Figure 28c), however, some nanoplates show stronger charge issues than the PPA-Halloysite under SEM, which is also an indication that a layer of polymer modification has been grafted on the surface.

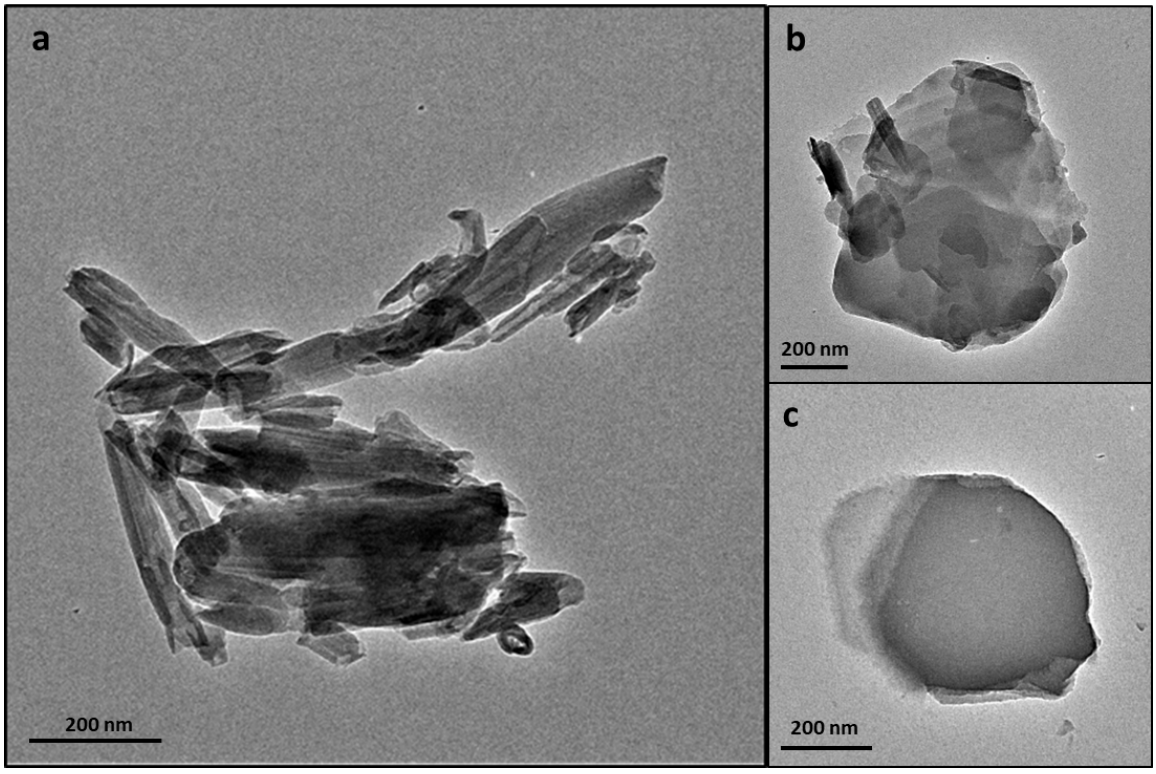

Figure 27. (a) TEM images of pristine Halloysite (b) PPA unfolded Halloysite nanoplate; (c) PPA-Halloysite-poly(DMAEMA) nanoplate surfactant.

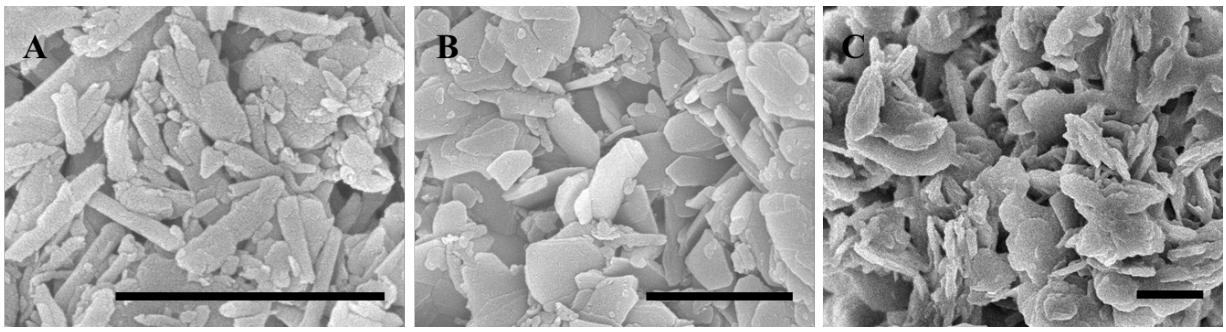

Figure 28. SEM images. A) raw Halloysite; B) PPA unfolded Halloysite nanoplatelet; C) PPA-Halloysite-Poly(DMAEMA) nanoplatelet surfactant.

3.4 Characterization of Janus Nanoplate Surfactant Stabilized Pickering Emulsion

3.4.1. Pickering Emulsions Stabilized by Janus Nanoplate Surfactants

Dodecane/water emulsion are generated with nanoplate surfactant and captured in a capillary tube to study the performance of Janus nanoplate surfactant. Figure 29a shows typical emulsion droplets stabilized by JNP surfactant. A uniform layer of platelets assembles at the emulsion interface even at a low surfactant concentration (0.25 weight % platelet concentration was used here). These Pickering emulsions exhibit a high polydispersity mainly due to the non-uniform size of the nanoplate produced from natural clay. Despite the large polydispersity observed from the microscopic image, emulsion droplets can remain stable against Ostwald ripening during a long period of time under high temperature (Figure 29a after 24 hours, 75 °C oven; fresh emulsion shown in Figure 30), which demonstrates the nanoplate surfactant's excellent ability to stabilize emulsions.

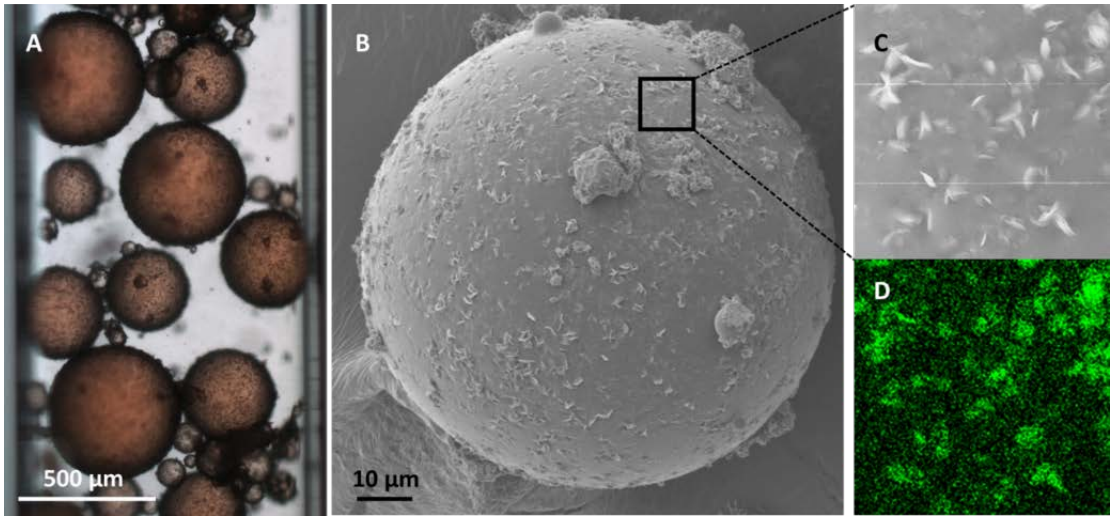

Figure 29. Pickering emulsion and interfaces: (A) Optical microscopic image of Dodecane in water emulsion: the emulsion is stabilized by Janus nanoplate surfactant. Dodecane oil is dyed with 0.1 wt% Sudan IV red. Emulsion is sealed in a square capillary tube with 1-mm side length for better observation purpose. Emulsion surface is covered by Janus nanoplate surfactant. (B) SEM image of polymerized styrene in water emulsion: emulsion droplet is stabilized by Janus nanoplate surfactant. The droplet shows a high surface coverage of Janus nanoplate surfactant. (C) Magnified view of emulsion surface. (D) EDS element mapping of the magnified region, which exhibits a strong signal of Al at the interface.

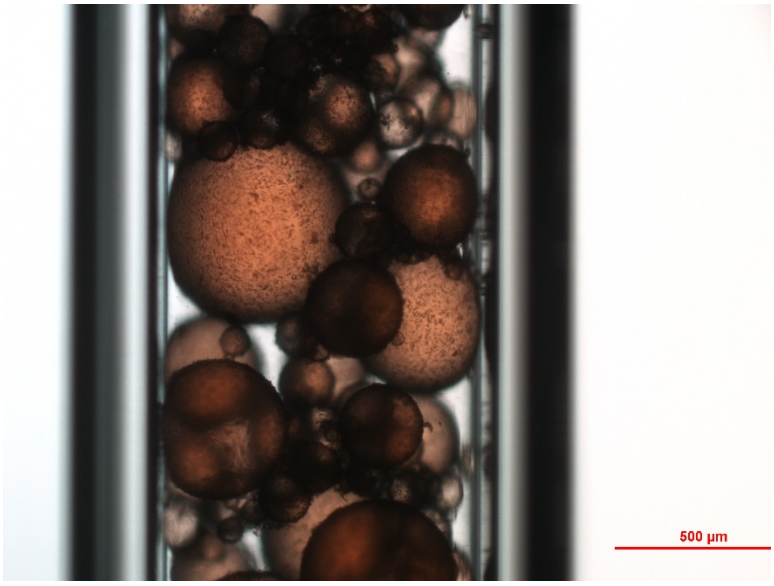

Figure 30. Fresh Dodecane/water emulsion stabilized by Janus nanoplate surfactant.

To better observe the platelet surfactant behavior at emulsion interface, we designed a polymerizable Pickering emulsion system. Firstly, a styrene/water emulsion was prepared with platelet surfactant as the only emulsifier. Then, by adding polymerization initiator and heating up emulsion in 80 °C oven, a styrene droplet was polymerized. The final polymerized styrene droplets stabilized with Janus platelets can be observed under normal SEM mode. The SEM image of polystyrene particles stabilized with nanoplate surfactant (Figure 29b) shows that, as surface active agent, Janus nanoplates are attached on the styrene water interface, forming a compact assembly to stabilized interface. There is no overlap between Janus nanoplates, which is consistent with spherical Janus system.[147,148] A magnified image (Figure 29c) at the interface shows that most nanoplates are parallel to the tangent direction of the interface, but some of the platelets are tilted. According to simulation work of other research teams,[26,60] those tilted and distorted configurations are thermodynamically unfavorable. The hypothesis is that platelets are tilted because of surface deformation, as a result of polymerization shrinkage during the polymerization of styrene. In comparison, one-side modified platelet, the PPA-Halloysite, fails to form stable emulsion droplets during polymerization (Figure 31), although it is able to form a Pickering emulsion of styrene in water before polymerization. The result shows that the asymmetric modification on the clay platelet is critical for it to emulsify and stabilize emulsions under high temperature (80 °C oven).

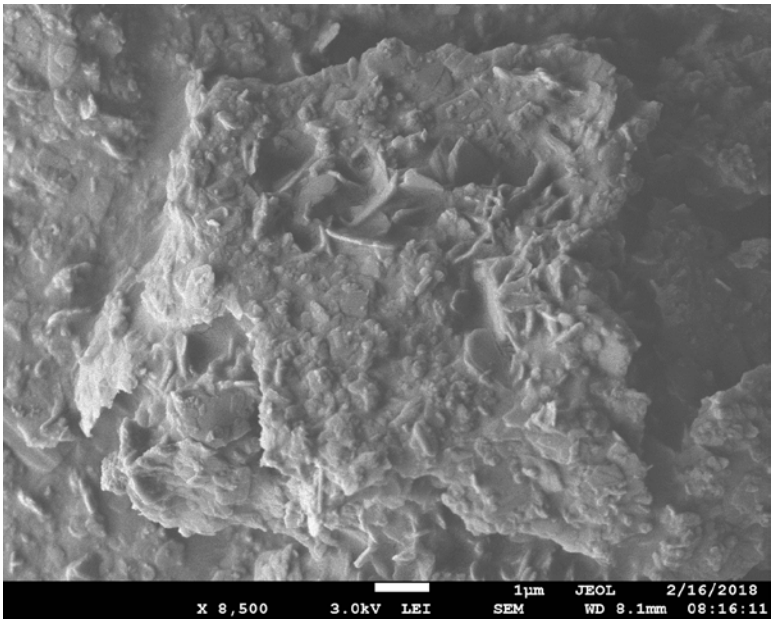

Figure 31. One-side modified nanoplates, PPA-Halloysite nanoplates, failed to stabilize styrene emulsions due to low surface activity. The spherical emulsion is destroyed during polymerization, which is carried out in a 75 °C oven for 12 hours. This comparison demonstrates the importance of double-side asymmetric modifications for emulsion stability under high temperature.

Energy dispersive spectroscopy (EDS) mapping is employed to further analyze platelet composition and distribution. The EDS mapping reveals the nanoplate attaching at the interface is mainly composed of Al, Si, O, and P (Figure 29d and Figure 32), which is consistent with the aluminosilicate based, PPA surface-modified nanoplate surfactant composition. Again, this result confirms the forming of platelet assembly layer at interface. Due to low contrast, some platelets at interface cannot be observed clearly with SEM image but can be seen on the EDS mapping.

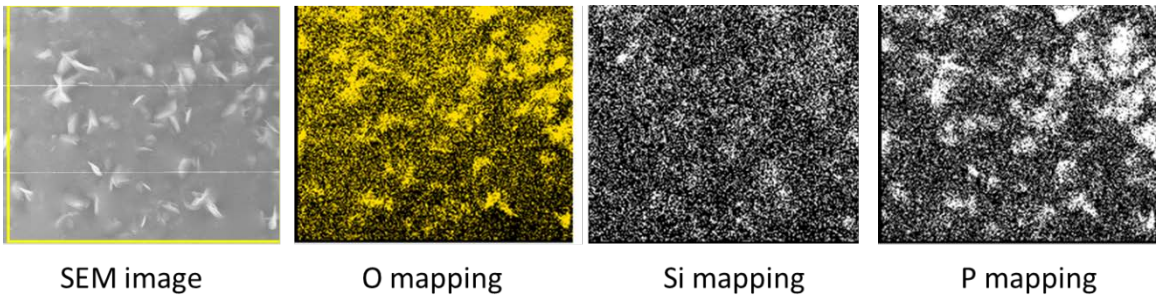

Figure 32. Energy-dispersive X-ray spectroscopy (EDS) element mapping of O, Si, P on polystyrene surface.

3.4.2. Salinity Tolerance of Nanoplate Surfactants Stabilized Pickering Emulsions

Salinity tolerance of the emulsion was also studied (Figure 33). Saline solution with different 5%, 10%, 15%, 20% weight concentration of calcium chloride was prepared. 0.25 w.t. % of modified Halloysite was used to emulsify Dodecane oil with different concertation of saline solutions, then solution was injected in pipette for phase volume observation. Results show that emulsions remain stable under 5% to 20% brine concentrations. Compared to Pickering emulsion stabilized by graphene, silica and other particles [149,150], Janus Halloysite surfactant demonstrates extraordinary salinity tolerance, which proved material is suitable for high salinity applications.

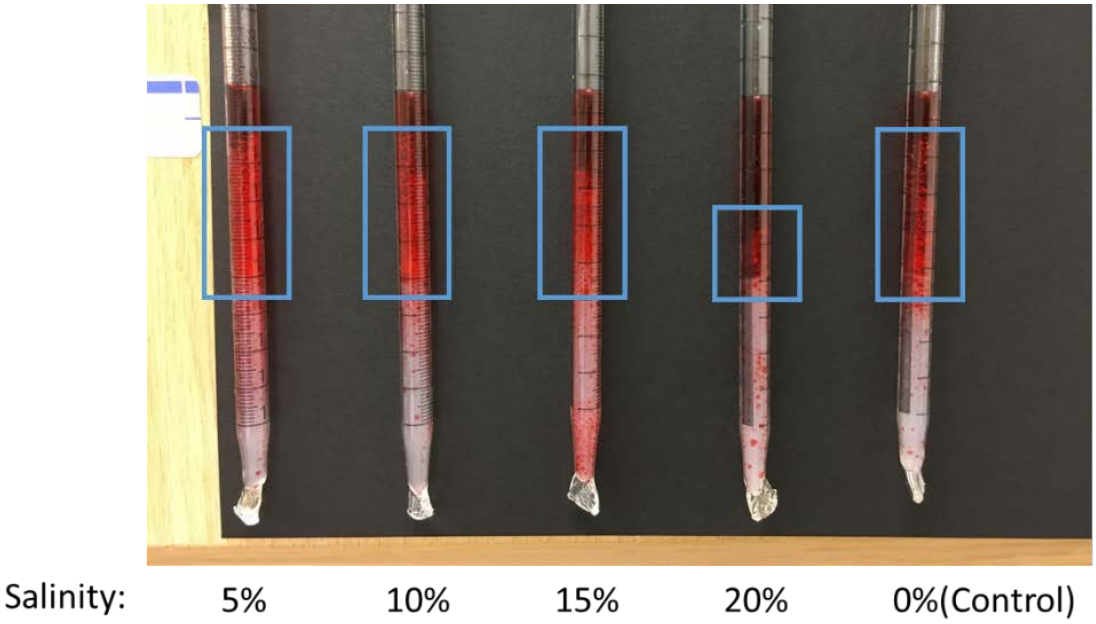

Figure 33. Nanoplate surfactant has a better performance under high salinity compared with conventional surfactants. Surfactant can still emulsify oil at 20% salinity and maintain a large quantity of emulsion at 15%.

3.4.3. Phase Behaviors of Oil/water Pickering Emulsion

Oil/water/nanoplate surfactant behaviors are studied under different compositions. Two capillary phases and an oil-in-water Pickering emulsion phase are observed in the emulsion system stabilized by the nanoplate surfactant, as shown in Figure 34 a and b. The two capillary phases correspond to oil forming a capillary phase with the hydrophobic platelet surface and water forming a capillary phase with the hydrophilic platelet surface, which is consistent with reports in the literature[151]. Dynamic interfacial tension is measured by the pendant drop method[146]. With 0.25 wt. % nanoplate surfactant, interfacial tension between Dodecane oil and water (Figure 34c) is dropping from 53.7 mN/m[152] to 47.0 ± 0.03 mN/m (equilibrium) within the measurement. On the contrast, platelets with hydrophobic modification on only one side drop from 53.7 mN/m to 49.0 ± 0.03mN/m

(equilibrium). Comparing these results, we find water/dodecane interfacial tension is reduced with the hydrophilic polymer modification on the silica side. IFT of lower concentration (0.1% and 0.2%) of Janus surfactant is also measured. Results show that IFT is proportional to Janus surfactant weight concentration. Compared to IFT data reported in other Pickering emulsion systems, such as bare silica particles and symmetrically modified silica particles[153,154], Janus nanoplates derived from Halloysite reduce IFT between oil and water the most.

Although, by itself, surface active nanoparticles cannot reduce IFT to the ultra-low level ($10^{-2}\ to\ 10^{-3}$ mN/m). The synergetic effect between molecular surfactant and nanoparticles has been observed by other researchers. With presence of 100 ppm ZrO_2, interfacial tension of SDS, crude oil and water is reduced from 16×10^{-3} mN/m to 3.1×10^{-3}mN/m.

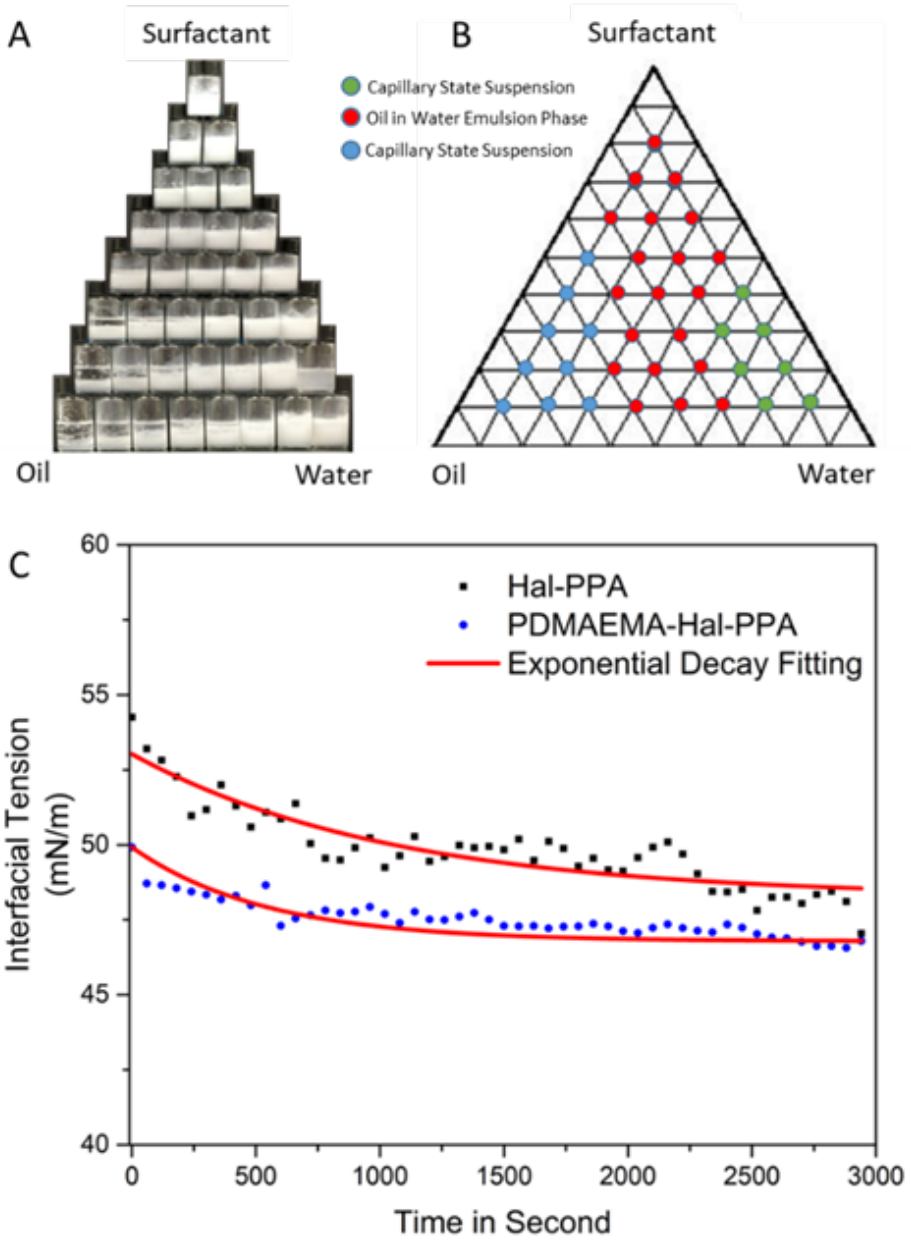

Figure 34. Phase behavior and interfacial tension: (A) Phase behavior of dodecane/water emulsion with 0.25 wt.% of Janus nanoplate surfactants. Surfactant, oil and water ratio change from 1 to 8. (B) Phase diagrams generated according to the equilibrium phase behavior. (C) Dynamic interfacial tension between dodecane and water, stabilized by Janus nanoplate surfactants and PPA-modified Halloysite platelets.

3.4.4. Enhanced Oil Recovery with Janus Nanoplate Surfactants

The chip flooding experiment was conducted with the set up shown in Figure 35a, and a part of the chip configuration is magnified and shown in Figure 35b. The flow rates of water and surfactant are both controlled at 0.2 ml/hour with a micro syringe pump. A maximum displacement of original oil in place, 31±3%, is achieved after 1 hour of water flooding. After that, 0.25 wt.% nanoplate surfactant suspension is injected into the chip again. After surfactant flooding, the total displacement of original oil in place is 52±3%, which means a 21±4% extra oil recovery is achieved with the Janus nanoplate surfactant (Figure 35e).

The improved oil displacement achieved by the Janus nanoplate surfactant is attributable to the emulsifiability of the platelet surfactant and the wettability alteration property of the nanoplate. We measured changes in contact angle induced by the nanoplates (Figure 35c and d). A glass substrate is first rendered hydrophobic with octyl triethoxysilane. The water droplet on the hydrophobic substrate contact angle is 101.0±5° initially. After flooding with Janus nanoplate surfactant and dried, the contact angle is reduced to 14.0±5°. The extraordinary oil displacement ratio observed during the chip flooding experiment can be attributed to Janus nanoplate's ability to alter wettability.

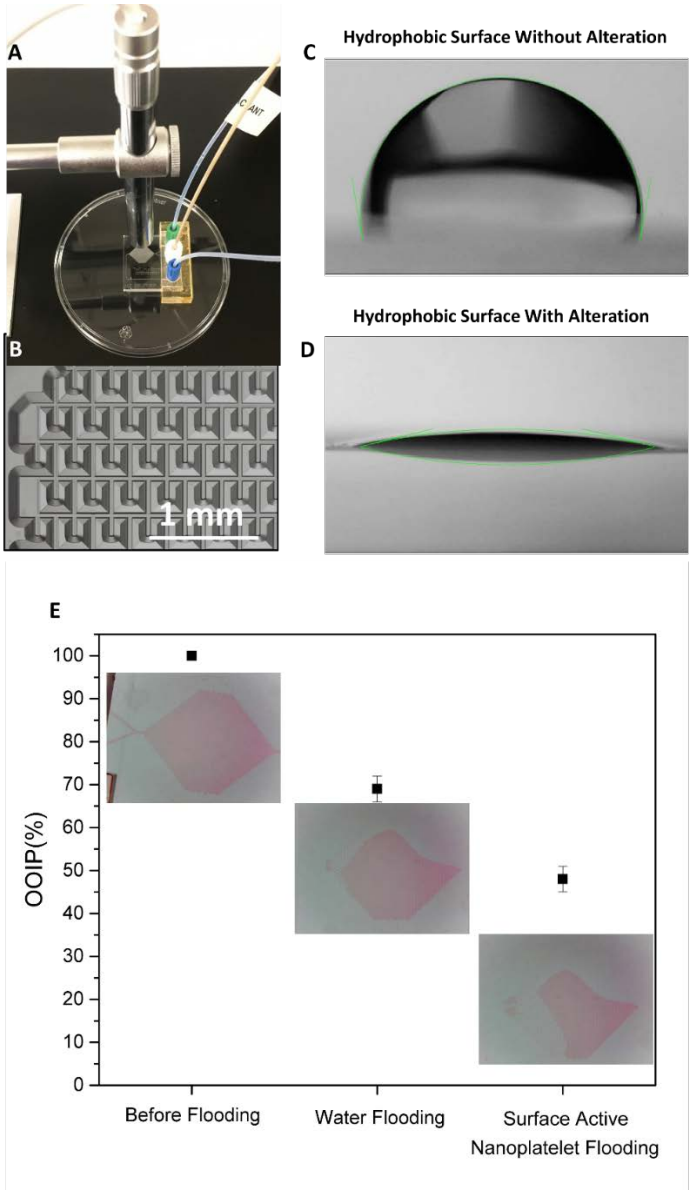

Figure 35. Flooding test and wettability alteration: (A) Water flooding and surfactant flooding test with microfluidics device. (B) A magnified image of microfluidics chip: the microfluidics chip has a pocket pattern with a 300µm × 300 µm square and a 150 µm × 20 µm groove in the middle. (C) Contact angle measurement of hydrophobic surface before wettability alteration. (D) Contact angle measurement of surface after wettability alteration. (E) Original oil in place (OOIP) changes after water flooding followed by surfactant flooding. With water flooding OOIP reaches 69%, and with further nanoplate surfactant flooding, the OOIP percentage improves to 48%.

3.4.5. Janus Nanoplate Surfactants Solid Surface Interaction

Wettability alteration was observed by contact angle measurement. However, not many researches explained the wettability alteration induced by surface modified nanoparticles, even less studied wettability alteration by Janus nanoplates, which possess distinct surface properties. A sand pack experiment was designed to simulate nanoflooding process with Janus nanoplate (Figure 36). Two glass pipes are connected with a flask clamp. A filter paper is inserted in between to hold sand. Silica sand is then added into the top part of the set-up and packed even. Sand pack is first rinsed with 8% octadecyl trimethoxy silane/heptane solution to render sand surface hydrophobic, then let solvent dry in the hood. 10 ml of Dodecane is transferred in the tube to saturate the oleophilic sand pack. 30 ml of 0.25 w.t.% Janus Halloysite and single-side modified Halloysite are added into tubes in two different trials to compare. After that, the sand grain from each trial are carefully dried and sampled for SEM observation.

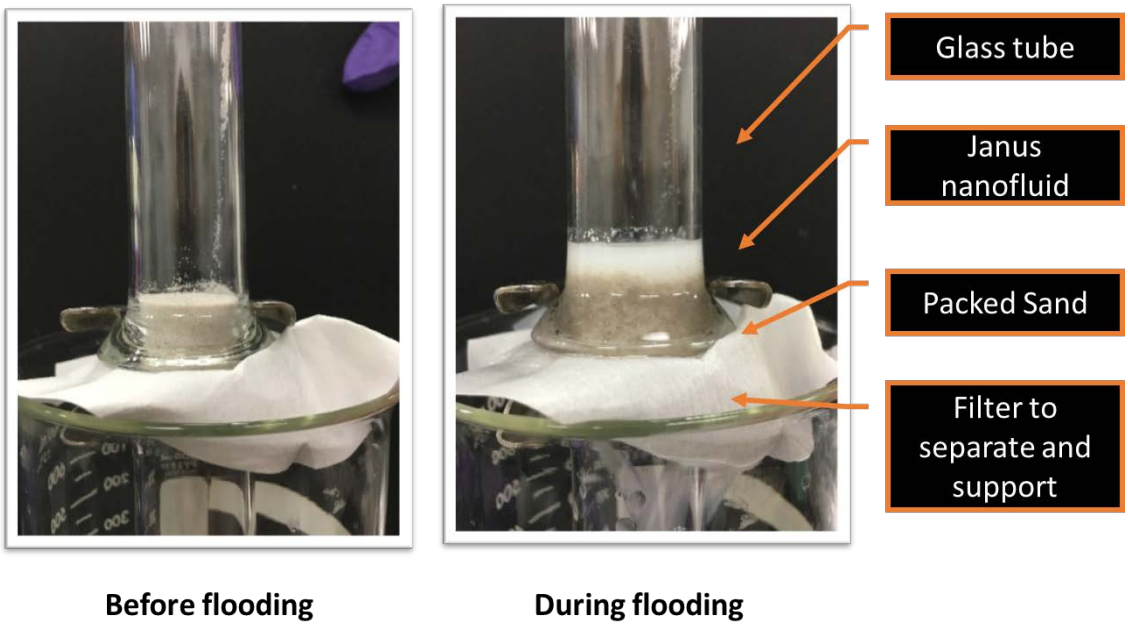

Figure 36. Sand pack model to study Janus nanoplate surfactants solid surface interaction. Left, Sand column with hydrophobic modification; Right, Sand column flooding with Janus nanoplate.

Samples of pristine silica sand (Figure 37), silica sand flooded with Janus Halloysite nanofluid (Figure 38 and Figure 39), and silica sand flooded with PPA Halloysite nanofluid (Figure 40) were exanimated under SEM. Figure 37 shows the pristine silica sand possesses a rough surface, but without impurity adsorption. After Janus Halloysite nanofluid flooding, the hydrophobic surface on the flow path is coated with a layer of nanoplates. A high magnification picture shows the lateral surface of nanomaterial attached on the sand surface. These platelets did not aggregate, but spread evenly to coverage rock surface.

The classical mechanism for molecular surfactant wettability alteration states that hydrophobic tail of surfactant would adsorb onto the oil-wet solid surface, and expose the hydrophilic head, resulting alteration of wettability[155]. This theory can be applied to the

Janus Halloysite nanofluid, because the Janus Halloysite surfactant also possess a hydrophilic side and hydrophobic side. When dispersed, these platelets are carried with aqueous phase and can diffuse into oil phase because of its amphiphilicity. The hydrophobic surface is then attached on the hydrophobic rock surface to form an energy favorable state, exposing the hydrophilic surface outside to change wettability and assist imbibition. Similar mechanism is also observed by Luo in amphiphilic graphene system[17]. A negative control experiment is conducted with single side PPA (hydrophobic) modified Halloysite. After nanofluid flooding, sand surface is observed under SEM. From Figure 40, we can see that PPA modified Halloysite were aggregated and scattered on the rock surface.

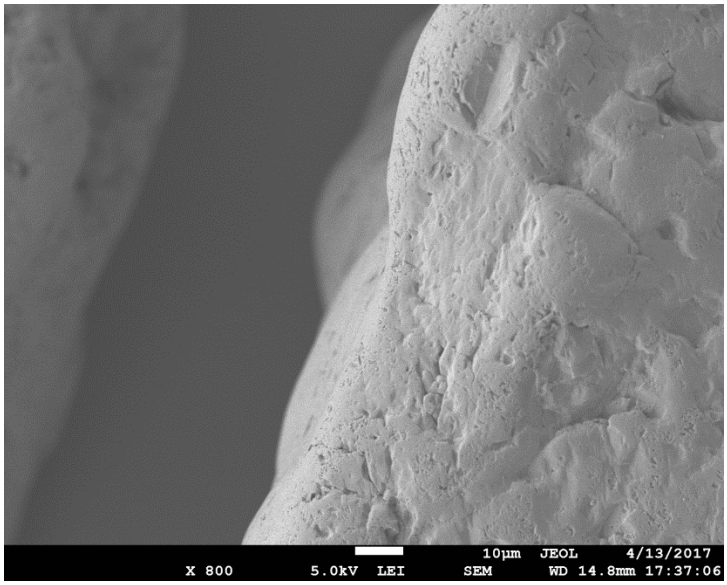

Figure 37. SEM of pristine silica sand.

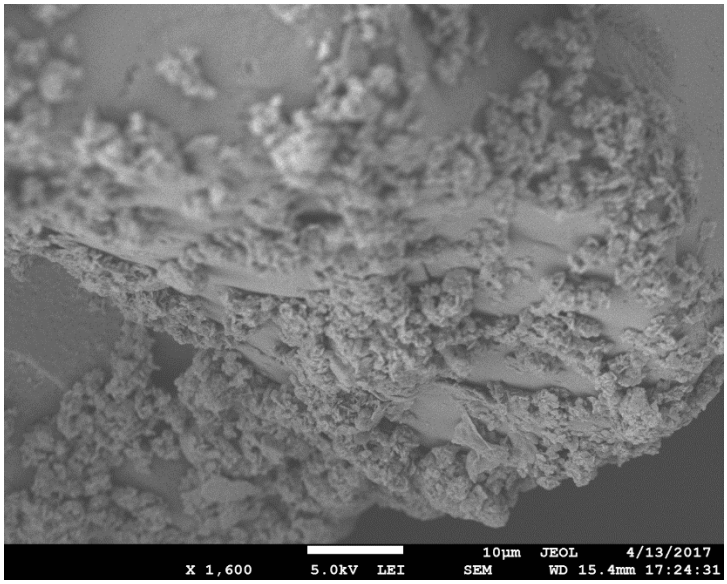

Figure 38. SEM of Janus nanoplate spreaded on hydrophobically modified silica surface after nanoflooding.

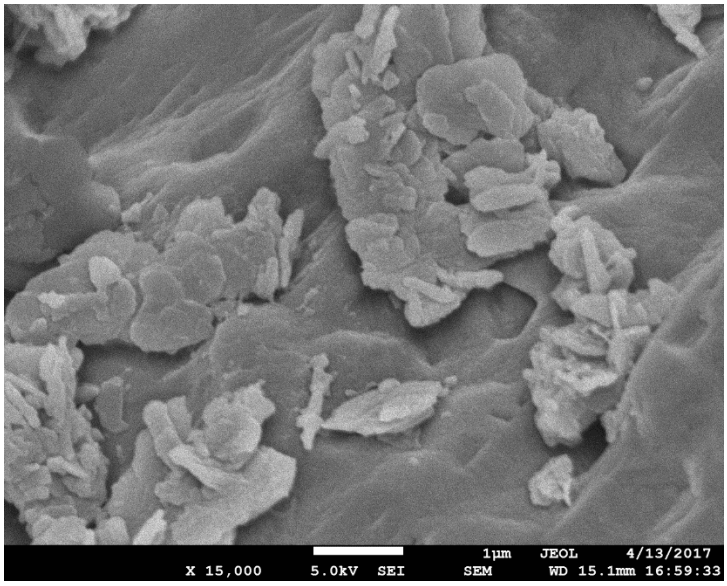

Figure 39. SEM picture at x15,000 magnification showing Janus nanoplate attached on silica surface.

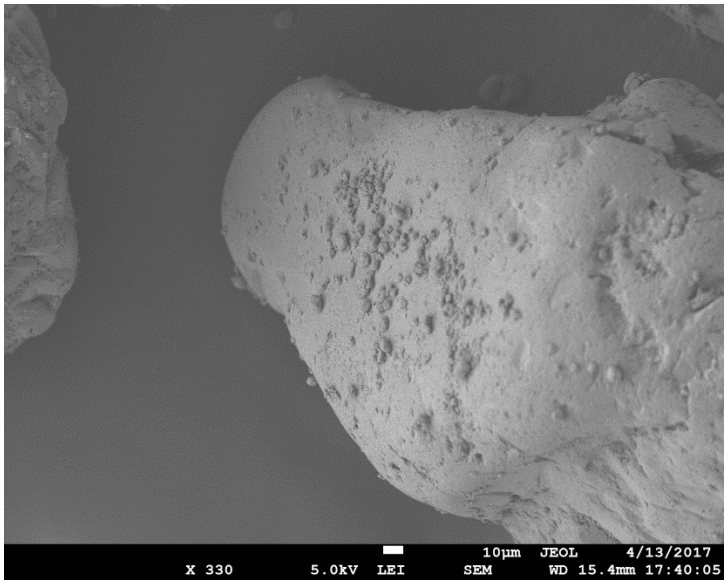

Figure 40. SEM of single side modified Halloysite on hydrophobically modified silica surface. Platelet aggregation is observed.

2.2. Summary of Chapter

Firstly, this chapter developed a unique method to prepare Janus nanoplates. By reacting PPA with Halloysite nanoscrolls, thin nanoplates were prepared. Surface initiated ATRP reaction was then designed to graft hydrophilic polymers on the silica side. After surface modifications on two side with hydrophilic and hydrophobic functional groups, Janus nanoplate surfactant was prepared. The synthesized material was then characterized with SEM, TEM, NMR and FT-IR to characterize morphology and confirm surface modification. From these results, it was concluded that alumina surface was modified with hydrophobic PPA and silica side was grafted with hydrophilic acrylate polymers.

Then, emulsion stability with Janus nanoplate surfactant was demonstrated with styrene/water emulsions. The styrene emulsion prepared with Janus nanoplate surfactant remained stable under high temperature, in contrast, styrene emulsion with single-side modified Halloysite coalesced in oven. This comparison illustrate that asymmetrical

surface modification is critical for nanoplate to stabilize emulsion under high temperature. Arrangement of nanoplates at emulsion interface was also studied by polymerizing styrene emulsion. Phase behavior and emulsion salinity tolerance of Janus nanoplate stabilized Pickering emulsion were also studied.

In the third part of this chapter, nanoflooding with Janus nanoplate surfactant was demonstrated on a microfluidic device. Enhanced OOIP recovery rate was observed, and explained with reduced IFT and surface wettability alteration. Wettability alteration was also demonstrated with contact angle and observation of sand grains under SEM.

CHAPTER IV

CONCLUSIONS AND FUTURE WORK

Conclusions

This dissertation focuses on developing different two dimensional nanoplates with various surface modifications through simple methodology, and employing such Janus nanoplate surfactant as nanofluid to demonstrate its potential application in enhance oil recovery. The potential opportunities and challenges of nanomaterial EOR are also discussed. The nanoflooding technique is expected to improve oil displacement efficiency to a large extent, and the research and development of nanomaterials-assisted EOR techniques have the potential to introduce revolutionary changes in the oil industry.

In the First Chapter, the theories related with nanofluid enhanced oil recovery has been reviewed. The benefit of nanoflooding could be concluded as wettability alteration, reducing interfacial tension, controllable viscosity, disjoint pressure for oil displacement and a stable foam and emulsion. Current progress in nanomaterial-assisted EOR has also been summarized in three categories according to material geometry: zero-dimensional, one-dimensional, and two dimensional. I compared oil emulsifiability of the different dimensions. According to simulation results and the thermal dynamic model, two-dimensional material seems to be the optimal candidate to generate stable emulsions. I concluded and assessed the properties of nanomaterials related to successful chemical EOR implementation, such as particle size, morphology, surface decoration and environment resistance, although the requirements for a successful nanoflooding EOR can vary case by case. Some general guidance for nanoflooding EOR is drawn. Nanoparticle

size, surface charge and nanomaterial structure should be evaluated before implementation to avoid formation damage and particle retention. Material morphology and surface functionalization should also be controlled to reduce interfacial tension. Material compatibility with formation conditions should also be evaluated before nanoflooding implementation to lower risks. In conclusion, the optimal nanomaterial for EOR should possess a discotic geometry with hydrophobic and hydrophilic surface modification on each side.

In the Second Chapter, several potential base material were investigated for Janus nanoplate synthesis. Because of its intrinsic asymmetry, Kaolin group material is selected as a base material for further surface modification. To acquire a thin layer of Kaolinite, exfoliation and bottom-up synthesis of Kaolinite have been explored, but were not successful. An alternative method was found by unscroll Halloysite tube structure. Thin Kaolin layer was obtained, and the hydrophobic modification was achieved at the same time.

In the Third Chapter, a facile method has been developed to produce Janus nanoplates in bulk reaction system with a two-step modification strategy, by choosing the natural Halloysite material as a model substrate. The asymmetric modifications of Janus nanoplates on both sides were characterized in detail. Such Janus nanoplates could function as colloidal surfactants, as they demonstrate an excellent performance in emulsification and emulsion stabilization. The phase behavior of the platelet surfactant system was explored, enabling the formation of emulsion phases by changing the oil/water/surfactant ratio. Furthermore, flooding experiment with the platelet surfactant

was carried out with microfluidic chips, achieving recovery of 21±4% extra oil due to the emulsifiability and wettability alteration of the nanoplate surfactant. This Janus nanoplate synthesis method greatly simplifies the manufacturing process of Janus nanoplate and makes mass production of Janus particle surfactants possible. The Janus platelet surfactant exhibits an excellent emulsifiability, emulsion stability, and ability alter surface wettability, which distinguishes it from conventional molecular surfactants for high-temperature and high-salinity applications. The research disclosed here not only provides important insights for the design and synthesis of Janus colloidal surfactant, but also creates opportunities for applications in areas of biomedical, food, mining and oil industries.

Future Work: Opportunities and Challenges

Application of nanomaterials in enhanced oil recovery has the potential to improve upstream productivity. Synthesis of different morphologies of nanomaterials is widely studied. Different surface modification methods have been reported. This dissertation reported methods to synthesize asymmetrically modified nanoplates for EOR application, but such nanomaterial can also be used for encapsulation and drug delivery. This dissertation only used micro channel chips for experiment. Core flooding should also be explored in future experiment. The detail mechanism of nanoflooding, however, is still being studied. More research effort should be addressed toward the study of interaction between nanomaterials and rock surface and oil/water interface. The stability of Pickering emulsions and foam has been proven both theoretically and experimentally, but thus far researchers have rarely applied those knowledge in nanomaterial enhanced oil recovery.

At present, the most successful applications of nanomaterials in oil field use are encapsulated breakers and tracers. Successful nanoflooding cases are only reported in laboratories. The author thinks nanoflooding is still at its infancy. More research on oil displacement mechanism and the behavior of nanoparticle at downhole can definitely accelerate the application of nanoflooding. The other factors limiting the wide application of nanomaterial in oil field use include cost and formation and environment risk assessment.

REFERENCES

1 Fletcher, A. and Davis, J., 2010, January. How EOR can be transformed by nanotechnology. In SPE improved oil recovery symposium. Society of Petroleum Engineers.

2 Kong, X. and Ohadi, M., 2010, January. Applications of micro and nano technologies in the oil and gas industry-overview of the recent progress. In Abu Dhabi international petroleum exhibition and conference. Society of Petroleum Engineers.

3 Kapusta, S., Balzano, L. and Te Riele, P.M., 2011. International Petroleum Technology Conference. Bangkok, Thailand, pp.15-17.

4 Li, L., Yuan, X., Xu, X., Li, S. and Wang, L., 2013, March. Vital role of nanotechnology and nanomaterials in the field of oilfield chemistry. In IPTC 2013: International Petroleum Technology Conference.

5 Ayatollahi, S. and Zerafat, M.M., 2012, January. Nanotechnology-assisted EOR techniques: New solutions to old challenges. In SPE international oilfield nanotechnology conference and exhibition. Society of Petroleum Engineers.

6 El-Diasty, A.I. and Aly, A.M., 2015, September. Understanding the mechanism of nanoparticles applications in enhanced oil recovery. In SPE North Africa technical conference and exhibition. Society of Petroleum Engineers.

7 Sheng, J. ed., 2013. Enhanced oil recovery field case studies. Gulf Professional Publishing.

8 McElfresh, P.M., Holcomb, D.L. and Ector, D., 2012, January. Application of nanofluid technology to improve recovery in oil and gas wells. In SPE international oilfield nanotechnology conference and exhibition. Society of Petroleum Engineers.

9 Negin, C., Ali, S. & Xie, Q. Application of nanotechnology for enhancing oil recovery–A review. *Petroleum* **2**, 324-333 (2016).

10 ShamsiJazeyi, H., Miller, C. A., Wong, M. S., Tour, J. M. & Verduzco, R. Polymer-Coated Nanoparticles for Enhanced Oil Recovery. *Journal of Applied Polymer Science* **131**, doi:ARTN 40576 10.1002/app.40576 (2014).

11 Dehghan Monfared, A., Ghazanfari, M. H., Jamialahmadi, M. & Helalizadeh, A. The Potential Application of Silica Nanoparticles for Wettability Alteration of Oil-Wet Calcite: A Mechanistic Study. *Energy & Fuels* (2016).

12 Karimi, A. *et al.* Wettability Alteration in Carbonates using Zirconium Oxide Nanofluids: EOR Implications. *Energy & Fuels* **26**, 1028-1036, doi:10.1021/ef201475u (2012).

13 Salehi, M., Johnson, S. J. & Liang, J. T. Mechanistic Study of Wettability Alteration Using Surfactants with Applications in Naturally Fractured Reservoirs. *Langmuir* **24**, 14099-14107, doi:10.1021/la802464u (2008).

14 Hirasaki, G. J., Miller, C. A. & Puerto, M. Recent Advances in Surfactant EOR. *Spe Journal* **16**, 889-907 (2011).

15 Standnes, D. C. & Austad, T. Wettability alteration in chalk 2. Mechanism for wettability alteration from oil-wet to water-wet using surfactants. *J Petrol Sci Eng* **28**, 123-143, doi:10.1016/s0920-4105(00)00084-x (2000).

16 Nwidee, L. N. *et al.* Nanoparticles influence on wetting behaviour of fractured limestone formation. *J Petrol Sci Eng* **149**, 782-788, doi:https://doi.org/10.1016/j.petrol.2016.11.017 (2017).

17 Luo, D. *et al.* Nanofluid of graphene-based amphiphilic Janus nanosheets for tertiary or enhanced oil recovery: High performance at low concentration. *Proceedings of the National Academy of Sciences*, 201608135 (2016).

18 Giraldo, J., Benjumea, P., Lopera, S., Cortés, F. B. & Ruiz, M. A. Wettability alteration of sandstone cores by alumina-based nanofluids. *Energy & Fuels* **27**, 3659-3665 (2013).

19 Maghzi, A., Mohammadi, S., Ghazanfari, M. H., Kharrat, R. & Masihi, M. Monitoring wettability alteration by silica nanoparticles during water flooding to heavy oils in five-spot systems: A pore-level investigation. *Experimental Thermal and Fluid Science* **40**, 168-176, doi:http://dx.doi.org/10.1016/j.expthermflusci.2012.03.004 (2012).

20 Wang, K., Wang, C., Sun, L. & Yi, F. in *Power and Energy Engineering Conference (APPEEC), 2010 Asia-Pacific.* 1-4 (IEEE).

21 Cheraghian, G. & Hendraningrat, L. A review on applications of nanotechnology in the enhanced oil recovery part A: effects of nanoparticles on interfacial tension. *International Nano Letters* **6**, 129-138 (2016).

22 Thomas, S., 2008. Enhanced oil recovery-an overview. Oil & Gas Science and Technology-Revue de l'IFP, 63(1), pp.9-19.

23 Sheng, J., 2010. Modern chemical enhanced oil recovery: theory and practice. Gulf Professional Publishing.

24 Glaser, N., Adams, D., Böker, A. & Krausch, G. Janus Particles at Liquid−Liquid Interfaces. *Langmuir* **22**, 5227-5229 (2006).

25 Cheng, Zhengdong, Andres F. Mejia, Agustin Diaz, Abraham Clearfield, Mahboobul S. Mannan, and Ya-Wen Chang. "Amphiphilic nanosheets and methods of making the same." U.S. Patent 9,586,983, issued March 7, 2017.

26 Xiang, W. *et al.* Amphiphilic nanosheet self-assembly at the water/oil interface: computer simulations. *Physical Chemistry Chemical Physics* **19**, 7576-7586 (2017).

27 de Gennes, P. G. Soft Matter (Nobel Lecture). *Angew Chem Int Edit* **31**, 842-845, doi:DOI 10.1002/anie.199208421 (1992).

28 Walther, A. & Müller, A. H. Janus particles: synthesis, self-assembly, physical properties, and applications. *Chem Rev* **113**, 5194-5261 (2013).

29 Ogolo, N.A. and Olafuyi, O.A., 2012. Onyekonwu MO Enhanced oil recovery using nanoparticles. The Society of Petroleum Engineers SPE.

30 Wasan, D. T. & Nikolov, A. D. Spreading of nanofluids on solids. *Nature* **423**, 156 (2003).

31 Wasan, D., Nikolov, A. & Kondiparty, K. The wetting and spreading of nanofluids on solids: Role of the structural disjoining pressure. *Current Opinion in Colloid & Interface Science* **16**, 344-349, doi:http://dx.doi.org/10.1016/j.cocis.2011.02.001 (2011).

32 Trokhymchuk, A., Henderson, D., Nikolov, A. & Wasan, D. T. A simple calculation of structural and depletion forces for fluids/suspensions confined in a film. *Langmuir* **17**, 4940-4947, doi:10.1021/la010047d (2001).

33 Zhang, H., Nikolov, A. & Wasan, D. Enhanced oil recovery (EOR) using nanoparticle dispersions: Underlying mechanism and imbibition experiments. *Energy & Fuels* **28**, 3002-3009 (2014).

34 Puerto, M., Hirasaki, G.J., Miller, C.A. and Barnes, J.R., 2012. Surfactant systems for EOR in high-temperature, high-salinity environments. SPE journal, 17(01), pp.11-19.

35 Espinoza, D.A., Caldelas, F.M., Johnston, K.P., Bryant, S.L. and Huh, C., 2010, January. Nanoparticle-stabilized supercritical CO2 foams for potential mobility control applications. In SPE Improved Oil Recovery Symposium. Society of Petroleum Engineers.

36 Sharma, T., Kumar, G. S., Chon, B. H. & Sangwai, J. S. Thermal stability of oil-in-water Pickering emulsion in the presence of nanoparticle, surfactant, and polymer. *J Ind Eng Chem* **22**, 324-334, doi:10.1016/j.jiec.2014.07.026 (2015).

37 Zhang, T., Davidson, D., Bryant, S.L. and Huh, C., 2010, January. Nanoparticle-stabilized emulsions for applications in enhanced oil recovery. In SPE improved oil recovery symposium. Society of Petroleum Engineers.

38 Zhang, T., Roberts, M., Bryant, S. L. & Huh, C. (Society of Petroleum Engineers).

39 Kim, J. W., Larsen, R. J. & Weitz, D. A. Synthesis of nonspherical colloidal particles with anisotropic properties. *J Am Chem Soc* **128**, 14374-14377, doi:10.1021/ja065032m (2006).

40 Park, J.-G., Forster, J. D. & Dufresne, E. R. High-yield synthesis of monodisperse dumbbell-shaped polymer nanoparticles. *J Am Chem Soc* **132**, 5960-5961 (2010).

41 Kim, J. W., Lee, D., Shum, H. C. & Weitz, D. A. Colloid surfactants for emulsion stabilization. *Adv. Mater.* **20**, 3239-+, doi:10.1002/adma.200800484 (2008).

42 Worthen, A. J. *et al.* Nanoparticle-stabilized carbon dioxide-in-water foams with fine texture. *J Colloid Interf Sci* **391**, 142-151, doi:http://dx.doi.org/10.1016/j.jcis.2012.09.043 (2013).

43 Zhang, T., Espinosa, D., Yoon, K.Y., Rahmani, A.R., Yu, H., Caldelas, F.M., Ryoo, S., Roberts, M., Prodanovic, M., Johnston, K.P. and Milner, T.E., 2011, January. Engineered nanoparticles as harsh-condition emulsion and foam stabilizers and as novel sensors. In Offshore Technology Conference. Offshore Technology Conference.

44 Adkins, S. S., Gohil, D., Dickson, J. L., Webber, S. E. & Johnston, K. P. Water-in-carbon dioxide emulsions stabilized with hydrophobic silica particles. *Physical Chemistry Chemical Physics* **9**, 6333-6343 (2007).

45 Espinoza, D.A., Caldelas, F.M., Johnston, K.P., Bryant, S.L. and Huh, C., 2010, January. Nanoparticle-stabilized supercritical CO2 foams for potential mobility control applications. In SPE Improved Oil Recovery Symposium. Society of Petroleum Engineers.

46 Yu, J., An, C., Mo, D., Liu, N. and Lee, R.L., 2012, January. Foam mobility control for nanoparticle-stabilized supercritical CO2 foam. In SPE improved oil recovery symposium. Society of Petroleum Engineers.

47 Guo, F. & Aryana, S. An experimental investigation of nanoparticle-stabilized CO2 foam used in enhanced oil recovery. *Fuel* **186**, 430-442, doi:http://dx.doi.org/10.1016/j.fuel.2016.08.058 (2016).

48 Skauge, Tormod, Kristine Spildo, and Arne Skauge. "Nano-sized particles for EOR." In SPE improved oil recovery symposium. Society of Petroleum Engineers, 2010.

49 Hendraningrat, L., Li, S. & Torsæter, O. A coreflood investigation of nanofluid enhanced oil recovery. *J Petrol Sci Eng* **111**, 128-138, doi:http://dx.doi.org/10.1016/j.petrol.2013.07.003 (2013).

50 Gulbis, J., King, M., Hawkins, G. & Brannon, H. Encapsulated breaker for aqueous polymeric fluids. *SPE production engineering* **7**, 9-14 (1992).

51 Samadzadeh, M., S. Hatami Boura, M. Peikari, S. M. Kasiriha, and A. Ashrafi. "A review on self-healing coatings based on micro/nanocapsules." Progress in Organic Coatings 68, no. 3 (2010): 159-164.

52 Bennetzen, Martin Vad, and Kristian Mogensen. "Novel applications of nanoparticles for future enhanced oil recovery." In International petroleum technology conference. International Petroleum Technology Conference, 2014.

53 Hu, H., Zhao, Z., Gogotsi, Y. & Qiu, J. Compressible Carbon Nanotube–Graphene Hybrid Aerogels with Superhydrophobicity and Superoleophilicity for Oil Sorption. *Environmental Science & Technology Letters* **1**, 214-220, doi:10.1021/ez500021w (2014).

54 Zhai, W., Li, G., Yu, P., Yang, L. & Mao, L. Silver phosphate/carbon nanotube-stabilized pickering emulsion for highly efficient photocatalysis. *The Journal of Physical Chemistry C* **117**, 15183-15191 (2013).

55 Shen, M. & Resasco, D. E. Emulsions Stabilized by Carbon Nanotube−Silica Nanohybrids. *Langmuir* **25**, 10843-10851, doi:10.1021/la901380b (2009).

56 Kusanagi, K., S. Murata, Y. Goi, M. Sabi, K. Zinno, Y. Kato, N. Togashi, T. Matsuoka, and Y. Liang. "Application of cellulose nanofiber as environment-friendly polymer for oil development." In SPE/IATMI Asia Pacific Oil & Gas Conference and Exhibition. Society of Petroleum Engineers, 2015.

57 Ehtesabi, H., Ahadian, M. M., Taghikhani, V. & Ghazanfari, M. H. Enhanced heavy oil recovery in sandstone cores using TiO_2 nanofluids. *Energy & Fuels* **28**, 423-430 (2013).

58 Kalashnikova, I., Bizot, H., Cathala, B. & Capron, I. New Pickering Emulsions Stabilized by Bacterial Cellulose Nanocrystals. *Langmuir* **27**, 7471-7479, doi:10.1021/la200971f (2011).

59 Kalashnikova, I., Bizot, H., Bertoncini, P., Cathala, B. & Capron, I. Cellulosic nanorods of various aspect ratios for oil in water Pickering emulsions. *Soft Matter* **9**, 952-959 (2013).

60 Gao, H.-M., Lu, Z.-Y., Liu, H., Sun, Z.-Y. & An, L.-J. Orientation and surface activity of Janus particles at fluid-fluid interfaces. *The Journal of Chemical Physics* **141**, 134907, doi:doi:http://dx.doi.org/10.1063/1.4897185 (2014).

61 Creighton, M. A., Ohata, Y., Miyawaki, J., Bose, A. & Hurt, R. H. Two-dimensional materials as emulsion stabilizers: interfacial thermodynamics and molecular barrier properties. *Langmuir* **30**, 3687-3696 (2014).

62 Kim, J. *et al.* Graphene Oxide Sheets at Interfaces. *J Am Chem Soc* **132**, 8180-8186, doi:10.1021/ja102777p (2010).

63 Mejia, A. F. *et al.* Pickering emulsions stabilized by amphiphilic nano-sheets. *Soft Matter* **8**, 10245-10245, doi:10.1039/c2sm25846c (2012).

64 Yu, Y.-H. & Cheng, Z. Nanoplatelet Surfactants for Enhanced Oil Recovery, in preparation.

65 Wang, X. *et al.* in *APS Meeting Abstracts.* 34012.

66 Guillot, S., Bergaya, F., de Azevedo, C., Warmont, F. & Tranchant, J.-F. Internally structured pickering emulsions stabilized by clay mineral particles. *J Colloid Interf Sci* **333**, 563-569 (2009).

67 Yang, F. *et al.* Pickering emulsions stabilized solely by layered double hydroxides particles: the effect of salt on emulsion formation and stability. *J Colloid Interf Sci* **302**, 159-169 (2006).

68 Rodriguez Pin, Elena, Matthew Roberts, Haiyang Yu, Chun Huh, and Steven Lawrence Bryant. "Enhanced migration of surface-treated nanoparticles in sedimentary rocks." In SPE annual technical conference and exhibition. Society of Petroleum Engineers, 2009.

69 Haase, M. F., Grigoriev, D., Moehwald, H., Tiersch, B. & Shchukin, D. G. Encapsulation of Amphoteric Substances in a pH-Sensitive Pickering Emulsion. *The Journal of Physical Chemistry C* **114**, 17304-17310, doi:10.1021/jp104052s (2010).

70 Golghanddashti, Hassan, Mohammad Saadat, Saeed Abbasi, and Abbas Shahrabadi. "Experimental investigation of water vaporization and its induced formation damage associated with underground gas storage." Journal of Porous Media 16, no. 2 (2013).

71 Amorim, C. *et al.* Effect of clay–water interactions on clay swelling by X-ray diffraction. *Nuclear Instruments and Methods in Physics Research Section A: Accelerators, Spectrometers, Detectors and Associated Equipment* **580**, 768-770 (2007).

72 Anderson, R. L. *et al.* Clay swelling — A challenge in the oilfield. *Earth-Science Reviews* **98**, 201-216, doi:http://dx.doi.org/10.1016/j.earscirev.2009.11.003 (2010).

73 Haraguchi, K. & Takehisa, T. Nanocomposite hydrogels: a unique organic-inorganic network structure with extraordinary mechanical, optical, and swelling/de-swelling properties. *Adv. Mater.* **14**, 1120 (2002).

74 Gonzalez, I. J. & Scherer, G. W. Effect of swelling inhibitors on the swelling and stress relaxation of clay bearing stones. *Environmental Geology* **46**, 364-377 (2004).

75 Singh, B. & Mackinnon, I. D. R. Experimental transformation of kaolinite to halloysite. *Clays and Clay Minerals* **44**, 825-834, doi:Doi 10.1346/Ccmn.1996.0440614 (1996).

76 Gardolinski, J. E. F. C. & Lagaly, G. Grafted organic derivatives of kaolinite: II. Intercalation of primary n-alkylamines and delamination. *Clay Minerals* **40**, 547-556, doi:10.1180/0009855054040191 (2005).

77 Kuroda, Y., Ito, K., Itabashi, K. & Kuroda, K. One-Step Exfoliation of Kaolinites and Their Transformation into Nanoscrolls. *Langmuir* **27**, 2028-2035, doi:Doi 10.1021/La1047134 (2011).

78 Hendraningrat, Luky, Li Shidong, and Ole Torsaeter. "A glass micromodel experimental study of hydrophilic nanoparticles retention for EOR project." In SPE Russian Oil and Gas Exploration and Production Technical Conference and Exhibition. Society of Petroleum Engineers, 2012.

79 Rege, S. & Fogler, H. A network model for deep bed filtration of solid particles and emulsion drops. *AIChE Journal* **34**, 1761-1772 (1988).

80 Zhang, Tiantian. "Modeling of nanoparticle transport in porous media." PhD diss., 2012.

81 Ahmadi, Milad, Ali Habibi, Peyman Pourafshari, and Shahabbodin Ayatollahi. "Zeta potential investigation and mathematical modeling of nanoparticles deposited on the rock surface to reduce fine migration." In SPE Middle East Oil and Gas Show and Conference. Society of Petroleum Engineers, 2011.

82 Dinsmore, A. D. *et al.* Colloidosomes: Selectively Permeable Capsules Composed of Colloidal Particles. *Science* **298**, 1006-1009, doi:10.1126/science.1074868 (2002).

83 de Folter, J. W. J. *et al.* Particle Shape Anisotropy in Pickering Emulsions: Cubes and Peanuts. *Langmuir* **30**, 955-964, doi:10.1021/la402427q (2014).

84 Madivala, B., Vandebril, S., Fransaer, J. & Vermant, J. Exploiting particle shape in solid stabilized emulsions. *Soft Matter* **5**, 1717-1727, doi:10.1039/B816680C (2009).

85 Hirasaki, G. J. Interpretation of the Change in Optimal Salinity With Overall Surfactant Concentration. doi:10.2118/10063-PA.

86 Alagic, E., Spildo, K., Skauge, A. & Solbakken, J. Effect of crude oil ageing on low salinity and low salinity surfactant flooding. *J Petrol Sci Eng* **78**, 220-227, doi:10.1016/j.petrol.2011.06.021 (2011).

87 Saien, J. & Akbari, S. Interfacial Tension of Toluene + Water + Sodium Dodecyl Sulfate from (20 to 50) °C and pH between 4 and 9. *Journal of Chemical & Engineering Data* **51**, 1832-1835, doi:10.1021/je060204g (2006).

88 Villers, D. & Platten, J. K. Temperature-Dependence of the Interfacial-Tension between Water and Long-Chain Alcohols. *J Phys Chem-Us* **92**, 4023-4024, doi:DOI 10.1021/j100325a005 (1988).

89 Vermolen, E. C. M., M. J. T. Van Haasterecht, and S. K. Masalmeh. "A systematic study of the polymer visco-elastic effect on residual oil saturation by core flooding." In SPE EOR Conference at Oil and Gas West Asia. Society of Petroleum Engineers, 2014.

90 Monfared, A. D., Ghazanfari, M. H., Jamialahmadi, M. & Helalizadeh, A. Adsorption of silica nanoparticles onto calcite: Equilibrium, kinetic, thermodynamic and DLVO analysis. *Chem Eng J* **281**, 334-344, doi:10.1016/j.cej.2015.06.104 (2015).

91 Binks, B. P. & Fletcher, P. D. I. Particles Adsorbed at the Oil−Water Interface: A Theoretical Comparison between Spheres of Uniform Wettability and “Janus” Particles. *Langmuir* **17**, 4708-4710, doi:10.1021/la0103315 (2001).

92 Kumar, A., Park, B. J., Tu, F. & Lee, D. Amphiphilic Janus particles at fluid interfaces. *Soft Matter* **9**, 6604-6617 (2013).

93 Takahara, Y. K. *et al.* Asymmetrically Modified Silica Particles: A Simple Particulate Surfactant for Stabilization of Oil Droplets in Water. *J Am Chem Soc* **127**, 6271-6275, doi:10.1021/ja043581r (2005).

94 Fernandez-Rodriguez, M. A. *et al.* Comparison of the Interfacial Activity between Homogeneous and Janus Gold Nanoparticles by Pendant Drop Tensiometry. *Langmuir* **30**, 1799-1804, doi:10.1021/la404194e (2014).

95 Taylor, R. *et al.* Small particles, big impacts: A review of the diverse applications of nanofluids. *Journal of Applied Physics* **113**, 19, doi:10.1063/1.4754271 (2013).

96 Felicia, L. J. & Philip, J. Effect of hydrophilic silica nanoparticles on the magnetorheological properties of ferrofluids: A study using opto-magnetorheometer. *Langmuir* **31**, 3343-3353 (2015).

97 Mahendran, V. & Philip, J. Non-enzymatic glucose detection using magnetic nanoemulsions. *Applied Physics Letters* **105**, 123110 (2014).

98 Zaibudeen, A. & Philip, J. Thermally tunable grating using thermo-responsive magnetic fluid. *Optical Materials* **66**, 117-121 (2017).

99 Taborda, E. A., Franco, C. A., Lopera, S. H., Alvarado, V. & Cortés, F. B. Effect of nanoparticles/nanofluids on the rheology of heavy crude oil and its mobility on porous media at reservoir conditions. *Fuel* **184**, 222-232 (2016).

100 Mehrali, M. *et al.* Investigation of thermal conductivity and rheological properties of nanofluids containing graphene nanoplatelets. *Nanoscale Res. Lett.* **9**, 12, doi:10.1186/1556-276x-9-15 (2014).

101 Yahya, N., Kashif, M., Nasir, N., Niaz Akhtar, M. & Yusof, N. M. in *Journal of Nano Research.* 115-126 (Trans Tech Publ).

102 Kothari, N., Raina, B., Chandak, K. B., Iyer, V. & Mahajan, H. P. (Society of Petroleum Engineers).

103 Gardolinski, J. E. F. C. & Lagaly, G. Grafted organic derivatives of kaolinite: I. Synthesis, chemical and rheological characterization. *Clay Minerals* **40**, 537-546, doi:10.1180/0009855054040190 (2005).

104 Kuroda, Y., Ito, K., Itabashi, K. & Kuroda, K. One-step exfoliation of kaolinites and their transformation into nanoscrolls. *Langmuir : the ACS journal of surfaces and colloids* **27**, 2028-2035, doi:10.1021/la1047134 (2011).

105 Hirsemann, D. *et al.* Large-scale, low-cost fabrication of Janus-type emulsifiers by selective decoration of natural kaolinite platelets. *Angewandte Chemie (International ed. in English)* **51**, 1348-1352, doi:10.1002/anie.201106710 (2012).

106 Weiss, S. *et al.* Hybrid Janus particles based on polymer-modified kaolinite. **54**, 1388-1396 (2013).

107 Hirsemann, D., Thomas, K. K., Wack, J., W, L. V. & Breu, J. Covalent Grafting to μ -Hydroxy-Capped Surfaces ? A Kaolinite Case Study. (2011).

108 Varadachari, C., Goswami, G. & Ghosh, K. Dissolution of iron oxides. *Clay Research* **25**, 1-22 (2006).

109 Kirillova, A. *et al.* Platelet Janus Particles with Hairy Polymer Shells for Multifunctional Materials. *ACS Appl. Mater. Interfaces* **6**, 13106-13114, doi:Doi 10.1021/Am502973y (2014).

110 Joussein, E. *et al.* Halloysite clay minerals- a review. doi:10.1180/0009855054040180 (2005).

111 Barrientos-Ramirez, S. *et al.* Surface modification of natural halloysite clay nanotubes with aminosilanes. Application as catalyst supports in the atom transfer radical polymerization of methyl methacrylate. *Appl Catal a-Gen* **406**, 22-33, doi:10.1016/j.apcata.2011.08.003 (2011).

112 Yah, W. O., Takahara, A. & Lvov, Y. M. Selective Modification of Halloysite Lumen with Octadecylphosphonic Acid: New Inorganic Tubular Micelle. *J Am Chem Soc* **134**, 1853-1859, doi:10.1021/ja210258y (2012).

113 Wei, Z., Wang, C., Liu, H., Zou, S. & Tong, Z. Halloysite nanotubes as particulate emulsifier: Preparation of biocompatible drug‐carrying PLGA microspheres based on pickering emulsion. *J Appl Polym Sci* **125** (2012).

114 Tang, Y. H. *et al.* Effects of unfolded and intercalated halloysites on mechanical properties of halloysite-epoxy nanocomposites. *Compos Part a-Appl S* **42**, 345-354, doi:10.1016/j.compositesa.2010.12.003 (2011).

115 Wypych, F. *et al.* Covalent grafting of phenylphosphonate groups onto layered silica derived from in situ-leached chrysotile fibers. *J. Mater. Chem.* **13**, 304-307 (2003).

116 Hong, L., Jiang, S. & Granick, S. Simple method to produce Janus colloidal particles in large quantity. *Langmuir* **22**, 9495-9499 (2006).

117 Pujari, S. P., Scheres, L., Marcelis, A. & Zuilhof, H. Covalent surface modification of oxide surfaces. *Angewandte Chemie International Edition* **53**, 6322-6356 (2014).

118 Raki, L. & Detellier, C. Lamellar organominerals: intercalation of phenylphosphonate into the layers of bayerite. *Chem. Commun.*, 2475-2476 (1996).

119 Thissen, P. *et al.* Activation of Surface Hydroxyl Groups by Modification of H-Terminated Si(111) Surfaces. *J Am Chem Soc* **134**, 8869-8874, doi:10.1021/ja300270w (2012).

120 Zeng, M. *et al.* The synthesis of amphiphilic luminescent graphene quantum dot and its application in miniemulsion polymerization. *Journal of Nanomaterials* **2016** (2016).

121 Dong, Y. *et al.* Blue luminescent graphene quantum dots and graphene oxide prepared by tuning the carbonization degree of citric acid. *Carbon* **50**, 4738-4743 (2012).

122 Sun, H. G., Zhang, J. C., Li, L., Xu, J. & Sun, D. J. Surface modification of natural Na-montmorillonite in alkane solvents using a quaternary ammonium surfactant. *Colloid Surface A* **426**, 26-32, doi:10.1016/j.colsurfa.2013.03.008 (2013).

123 Ruzicka, B. & Zaccarelli, E. A fresh look at the Laponite phase diagram. *Soft Matter* **7**, 1268-1286, doi:10.1039/c0sm00590h (2011).

124 Vol. #AEO2017 (ed Department of Energy Energy Information Administration) (2017).

125 Peng, B. *et al.* A review of nanomaterials for nanofluid enhanced oil recovery. *RSC Advances* **7**, 32246-32254 (2017).

126 Leal-Calderon, F., Bibette, J. & Schmitt, V. in *Emulsion Science: Basic Principles* 143-172 (Springer New York, 2007).

127 Cunningham, V. J. *et al.* Giant Pickering Droplets: Effect of Nanoparticle Size and Morphology on Stability. *Langmuir* **33**, 7669-7679, doi:10.1021/acs.langmuir.7b01383 (2017).

128 Qi, L. *et al.* Segregation of Amphiphilic Polymer-Coated Nanoparticles to Bicontinuous Oil/Water Microemulsion Phases. *Energy & Fuels* **31**, 1339-1346 (2017).

129 Murray, B. S., Durga, K., Yusoff, A. & Stoyanov, S. D. Stabilization of foams and emulsions by mixtures of surface active food-grade particles and proteins. *Food Hydrocolloid* **25**, 627-638, doi:10.1016/j.foodhyd.2010.07.025 (2011).

130 Dickinson, E. Food emulsions and foams: Stabilization by particles. *Current Opinion in Colloid & Interface Science* **15**, 40-49, doi:10.1016/j.cocis.2009.11.001 (2010).

131 Schramm, L. L. *Emulsions, foams, and suspensions: fundamentals and applications*. (John Wiley & Sons, 2006).

132 Nguyen, A. & Schulze, H. J. *Colloidal science of flotation*. Vol. 118 (CRC Press, 2003).

133 Chevalier, Y. & Bolzinger, M.-A. Emulsions stabilized with solid nanoparticles: Pickering emulsions. *Colloids and Surfaces A: Physicochemical and Engineering Aspects* **439**, 23-34 (2013).

134 Gers-Barlag, Heinrich, Anja Müller, Xenia Petsitis, Ghita Lanzendörfer, and Melanie Kovacevic. "Hydrous cosmetic or pharmaceutical sticks." U.S. Patent 7,037,511, issued May 2, 2006.

135 Grishkewich, N., Mohammed, N., Tang, J. T. & Tam, K. C. Recent advances in the application of cellulose nanocrystals. *Current Opinion in Colloid & Interface Science* **29**, 32-45, doi:10.1016/j.cocis.2017.01.005 (2017).

136 Briggs, N. *et al.* Stable pickering emulsions using multi-walled carbon nanotubes of varying wettability. *Colloids and Surfaces A: Physicochemical and Engineering Aspects* **537**, 227-235, doi:https://doi.org/10.1016/j.colsurfa.2017.10.010 (2018).

137 Brunier, B., Sheibat-Othman, N., Chniguir, M., Chevalier, Y. & Bourgeat-Lami, E. Investigation of Four Different Laponite Clays as Stabilizers in Pickering Emulsion Polymerization. *Langmuir* **32**, 6046-6057, doi:10.1021/acs.langmuir.6b01080 (2016).

138 Ashby, N. & Binks, B. Pickering emulsions stabilised by Laponite clay particles. *Physical Chemistry Chemical Physics* **2**, 5640-5646 (2000).

139 Voorn, D. J., Ming, W. & van Herk, A. M. Polymer−Clay Nanocomposite Latex Particles by Inverse Pickering Emulsion Polymerization Stabilized with Hydrophobic Montmorillonite Platelets. *Macromolecules* **39**, 2137-2143, doi:10.1021/ma052539t (2006).

140 Levine, S., Bowen, B. D. & Partridge, S. J. Stabilization of emulsions by fine particles I. Partitioning of particles between continuous phase and oil/water interface. *Colloids and Surfaces* **38**, 325-343, doi:https://doi.org/10.1016/0166-6622(89)80271-9 (1989).

141 Aveyard, R., Binks, B. P. & Clint, J. H. Emulsions stabilised solely by colloidal particles. *Adv Colloid Interfac* **100**, 503-546, doi:Pii S0001-8686(02)00069-6

Doi 10.1016/S0001-8686(02)00069-6 (2003).

142 Guevara, J. S. *et al.* Stabilization of Pickering foams by high-aspect-ratio nano-sheets. *Soft Matter* **9**, 1327-1336, doi:Doi 10.1039/C2sm27061g (2013).

143 Lattuada, M. & Hatton, T. A. Synthesis, properties and applications of Janus nanoparticles. *Nano Today* **6**, 286-308, doi:10.1016/j.nantod.2011.04.008 (2011).

144 Zhang, L. *et al.* Janus graphene from asymmetric two-dimensional chemistry. *Nat Commun* **4**, 1443, doi:10.1038/ncomms2464 https://www.nature.com/articles/ncomms2464#supplementary-information (2013).

145 Stöter, M. *et al.* Controlled Exfoliation of Layered Silicate Heterostructures into Bilayers and Their Conversion into Giant Janus Platelets. *Angewandte Chemie* **128**, 7524-7528, doi:10.1002/ange.201601611 (2016).

146 Berry, J. D., Neeson, M. J., Dagastine, R. R., Chan, D. Y. & Tabor, R. F. Measurement of surface and interfacial tension using pendant drop tensiometry. *J Colloid Interf Sci* **454**, 226-237 (2015).

147 Chai, Y., Lukito, A., Jiang, Y., Ashby, P. D. & Russell, T. P. Fine-Tuning Nanoparticle Packing at Water–Oil Interfaces Using Ionic Strength. *Nano Lett.* **17**, 6453-6457, doi:10.1021/acs.nanolett.7b03462 (2017).

148 Lin, Y., Skaff, H., Emrick, T., Dinsmore, A. & Russell, T. P. Nanoparticle assembly and transport at liquid-liquid interfaces. *Science* **299**, 226-229 (2003).

149 AfzaliTabar, M. *et al.* Facile and economical preparation method of nanoporous graphene/silica nanohybrid and evaluation of its Pickering emulsion properties for Chemical Enhanced oil Recovery (C-EOR). *Fuel* **206**, 453-466, doi:https://doi.org/10.1016/j.fuel.2017.05.102 (2017).

150 Qi, L. *et al.* Segregation of Amphiphilic Polymer-Coated Nanoparticles to Bicontinuous Oil/Water Microemulsion Phases. *Energy & Fuels* **31**, 1339-1346, doi:10.1021/acs.energyfuels.6b02687 (2017).

151 Velankar, S. S. A non-equilibrium state diagram for liquid/fluid/particle mixtures. *Soft Matter* **11**, 8393-8403 (2015).

152 Zeppieri, S., Rodríguez, J. & López de Ramos, A. L. Interfacial Tension of Alkane + Water Systems. *Journal of Chemical & Engineering Data* **46**, 1086-1088, doi:10.1021/je000245r (2001).

153 Frelichowska, J., Bolzinger, M.-A. & Chevalier, Y. Pickering emulsions with bare silica. *Colloids and Surfaces A: Physicochemical and Engineering Aspects* **343**, 70-74, doi:https://doi.org/10.1016/j.colsurfa.2009.01.031 (2009).

154 Vignati, E., Piazza, R. & Lockhart, T. P. Pickering Emulsions: Interfacial Tension, Colloidal Layer Morphology, and Trapped-Particle Motion. *Langmuir* **19**, 6650-6656, doi:10.1021/la034264l (2003).

155 Hammond, P. S. & Unsal, E. Spontaneous imbibition of surfactant solution into an oil-wet capillary: wettability restoration by surfactant− contaminant complexation. *Langmuir* **27**, 4412-4429 (2011).

156 Penny, Glenn S., John Thomas Pursley, and David Holcomb. "The application of microemulsion additives in drilling and stimulation results in enhanced gas production." In SPE Production Operations Symposium. Society of Petroleum Engineers, 2005.

157 Tudor, Eric Hughson, Grant Walter Nevison, Sean Allen, and Blaine Pike. "100% gelled LPG fracturing process: an alternative to conventional water-based fracturing techniques." In SPE Eastern Regional Meeting. Society of Petroleum Engineers, 2009.

158 Grassman, D. & Zingg, W. (Google Patents, 1974).

159 Samuel, M. M. *et al.* Polymer-free fluid for fracturing applications. *Spe Drill Completion* **14**, 240-246 (1999).

160 Deng, Q., Xu, J. F., Gu, X. F. & Tang, Y. Properties Evaluation of Polymer-free Fluid for Fracturing Application. *Advanced Composite Materials, Pts 1-3* **482-484**, 1180-1183, doi:10.4028/www.scientific.net/AMR.482-484.1180 (2012).

161 Pursley, J. T., Penny, G. & Holcomb, D. in *SPE International Symposium and Exhibition on Formation Damage Control.* (Society of Petroleum Engineers).

162 Kim, J., Gomaa, A. M., Nelson, S. G. & Hudson, H. G. in *SPE International Conference and Exhibition on Formation Damage Control.* (Society of Petroleum Engineers).

163 Bui, Khoa, I. Yucel Akkutlu, Andrei Zelenev, Hasnain Saboowala, John R. Gillis, and James A. Silas. "Insights into mobilization of shale oil by use of microemulsion." SPE Journal 21, no. 02 (2016): 613-620.

164 Liu, D. X., Fan, M. F., Yao, L. T., Zhao, X. T. & Wang, Y. L. A new fracturing fluid with combination of single phase microemulsion and gelable polymer system. *J Petrol Sci Eng* **73**, 267-271, doi:DOI 10.1016/j.petrol.2010.07.008 (2010).

165 He, K., Xu, L., Gao, Y. F., Yin, X. L. & Neeves, K. B. Evaluation of surfactant performance in fracturing fluids for enhanced well productivity in unconventional reservoirs using Rock-on-a-Chip approach. *J Petrol Sci Eng* **135**, 531-541, doi:10.1016/j.petrol.2015.10.008 (2015).

166 Penny, Glenn S., Terrell Allen Dobkins, and John Thomas Pursley. "Field study of completion fluids to enhance gas production in the Barnett Shale." In SPE gas technology symposium. Society of Petroleum Engineers, 2006.

167 Dantas, T. N. C., Santanna, V. C., Neto, A. A. D., Neto, E. L. B. & Moura, M. C. P. A. Rheological properties of a new surfactant-based fracturing gel. *Colloid Surface A* **225**, 129-135, doi:10.1016/S0927-7757(03)00355-8 (2003).

168 Sihler, S., Schrade, A., Cao, Z., & Ziener, U. (2015). Inverse Pickering emulsions with droplet sizes below 500 nm. *Langmuir*, *31*(38), 10392-10401.

APPENDIX A

A SYSTEMATIC STUDY ON SHEAR-TOLERANT MICRO-EMULSION FRACTURING FLUID

A.1. Summary

Fluid loss control, formation damage prevention and mitigation are critical problems that affect hydraulic fracturing productivity in the low permeability gas reservoirs. In this work, we propose that micro-emulsion fracturing fluids should be used to reduce fluid loss and avoid formation damage. We used the Winsor IV single phase micro-emulsions, emulsified by non-ionic surfactants and co-surfactants, as emulsion component. Then mixed the emulsion with Guar Gum component, formulated a micro-emulsion fracturing fluid. Different parameters of formulated system, including gelation times, shearing tolerance at high temperature, fluid loss, formation damage and pipe friction were evaluated to characterize this novel fracturing fluid. With comprehensive measurements and evaluations, along with comparison to the conventional fracturing fluids, we have demonstrated that the micro-emulsion fracturing fluid has less fluid loss, controllable formation damage and it can still maintain a high viscosity under high temperature for a long period. The proposed micro-emulsion fracturing fluids have the potential to solve fluid loss and formation damage problems which are bothering high temperature formation fracturing treatment in low permeability formations.

A.2. Introduction

Undoubtedly, hydraulic fracturing technique and horizontal drilling techniques have changed the landscape of the world's energy production. Successful applications of hydraulic fracturing technique on the unconventional shale gas formations are helping the U.S. increase energy production and decrease energy import, meanwhile creating thousands of jobs. However, innovations for fracturing operations are still demanded to reduce cost, increase well life time and secure energy supply for centuries.

Fluid loss and formation damage are two factors limiting fracturing operations since it was developed [156]. Fluid loss results in a requirement for a tremendous amount of water to complete a fracturing treatment, which puts hydraulic fracturing under controversy and also increases cost of fracturing operation. The second factor, formation damage, reduces formation permeability, which limits well lifetime and undermines productivity.

Several new technologies have been proposed to solve these problems, such as critical state CO_2 or liquefied petroleum gas (LPG) [157,158]. One drawback of such techniques is that they are utterly different from the conventional fracturing process, thus costing more to modify the current equipment. Visco-Elastic surfactants (VES) fracture [159,160] is another new technology developed to fix fluid loss. However, under high temperature and high shear rate conditions, fluid viscosity would be compromised, besides the high cost of VES.

Micro-emulsions, which have already been widely applied in upstream, are mixtures of oil and water with surfactants [161-163]. Applications of micro-emulsions/gel as fracturing fluids were reported by other groups [164-166]. By altering wettability of pore throat, micro-emulsion can hydrophobize rock surface and reduce capillary pressure. A lower capillary pressure is preferred in anyways, from increasing productivity to reduce trapped fluid phase. In addition, benefited from the fact that micro-emulsion fracturing fluids are still homogeneous liquid phase under ambient temperature and pressure, instruments for conventional fluids can also implement micro-emulsion fracturing fluids with minor changes, which avoids cost for new treatment systems. Last but not least, micro-emulsion has a higher surface volume ratio compared to macro-emulsion system. By virtue of large surface volume ratio, emulsion droplets has higher chance to contact with rock surface hence alter the wettability. Also diesel usage in the fluids is also reduced by the large surface volume ratio, which renders the diesel fracturing fluid as an economy method for fracturing.

Here we present a systematic investigation on applying micro-emulsion based fracturing fluids to reduce fluid loss and formation damage. To obtain a stable emulsion, we screened different compositions of water, oil and surfactants. With the aid of a ternary phase diagram, we located the stable Winsor IV phase micro-emulsions. Based on that, we developed micro-emulsion fracturing fluids. Fluid rheology is the most Crucial parameters for fracturing fluids [167]. In our work, fluid rheological properties were measured and formation damage was evaluated with synthetic core samples. Experiment results showed that the new micro-fracturing fluids can maintain a high viscosity under high shearing rate and high temperature. Further investigations on micro-emulsion fracturing system also showed a reduced formation damage and fluid loss.

A.3. Result and Discussion

A.3.1 Phase Behavior

We used diesel as a model oil phase to explore the phase behaviors of the micro-emulsion fracturing fluids, even though EPA has strict rules on diesel fracking operation due to drinking water safety concern. Blended surfactant serving as an emulsifier was obtained

by mixing primary surfactant Triton-X 100 with co-surfactant n-Butanol under magnetic stirring in 2:1 mass ratio. The mixture was then stocked for later use. A through phase behavior study was carried out to locate an optimal composition for the micro-emulsion fracturing fluids. Results are shown in Figure 41 and Figure 42. Formula for the single phase micro-emulsion (Winsor IV in Figure 42) can be obtained by mixing emulsifier, diesel and water in a 0.5:69.65: 29.85 weight ratio. The micro-emulsions are thermodynamically equilibrium phase and very stable. A batch of 6 months old samples were compared with samples shown in Figure 42 and barely changed. Micro-emulsion forms spontaneously and requires no external energy input. A uniform single phase micro-emulsion can be acquired simply by shaking the sample vials with hand.

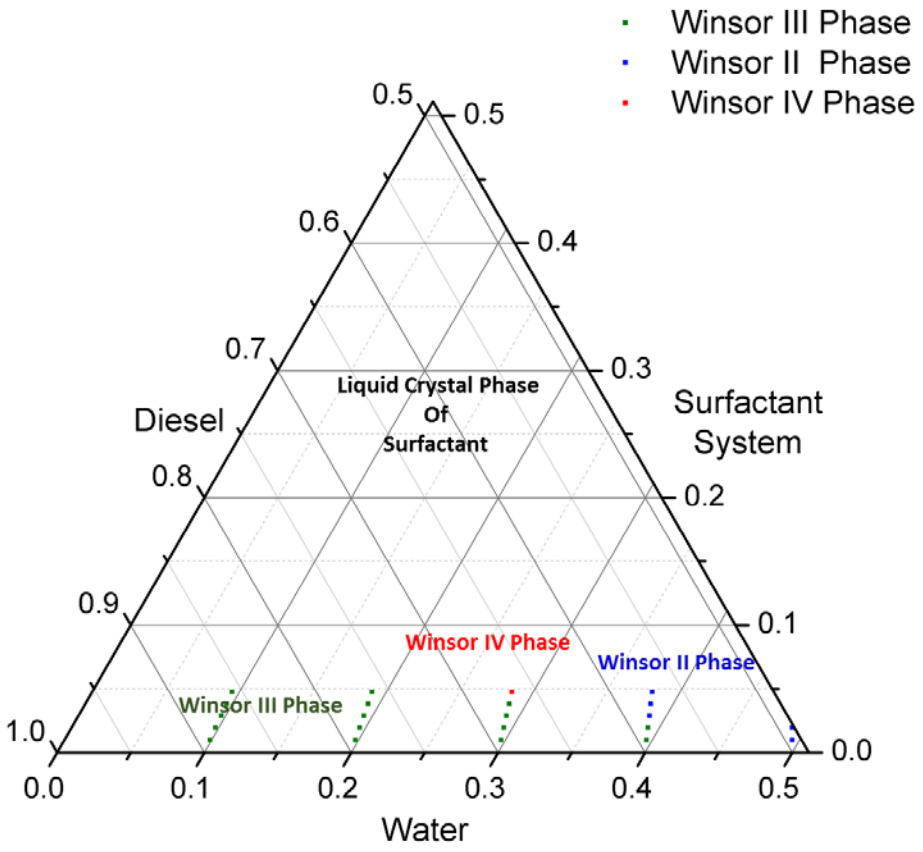

Figure 41. A tertiary phase diagram of Triton-X 100/n-Butanol, Diesel, Water mixture (zoomed into the Diesel corner). Compositions are labeled in weight ratio. Different color indicates the different Winsor phase type, see legend. Winsor II, III, IV phases were observed. The formulation of micro-emulsion fracturing fluids is based on the composition of Winsor IV emulsions.

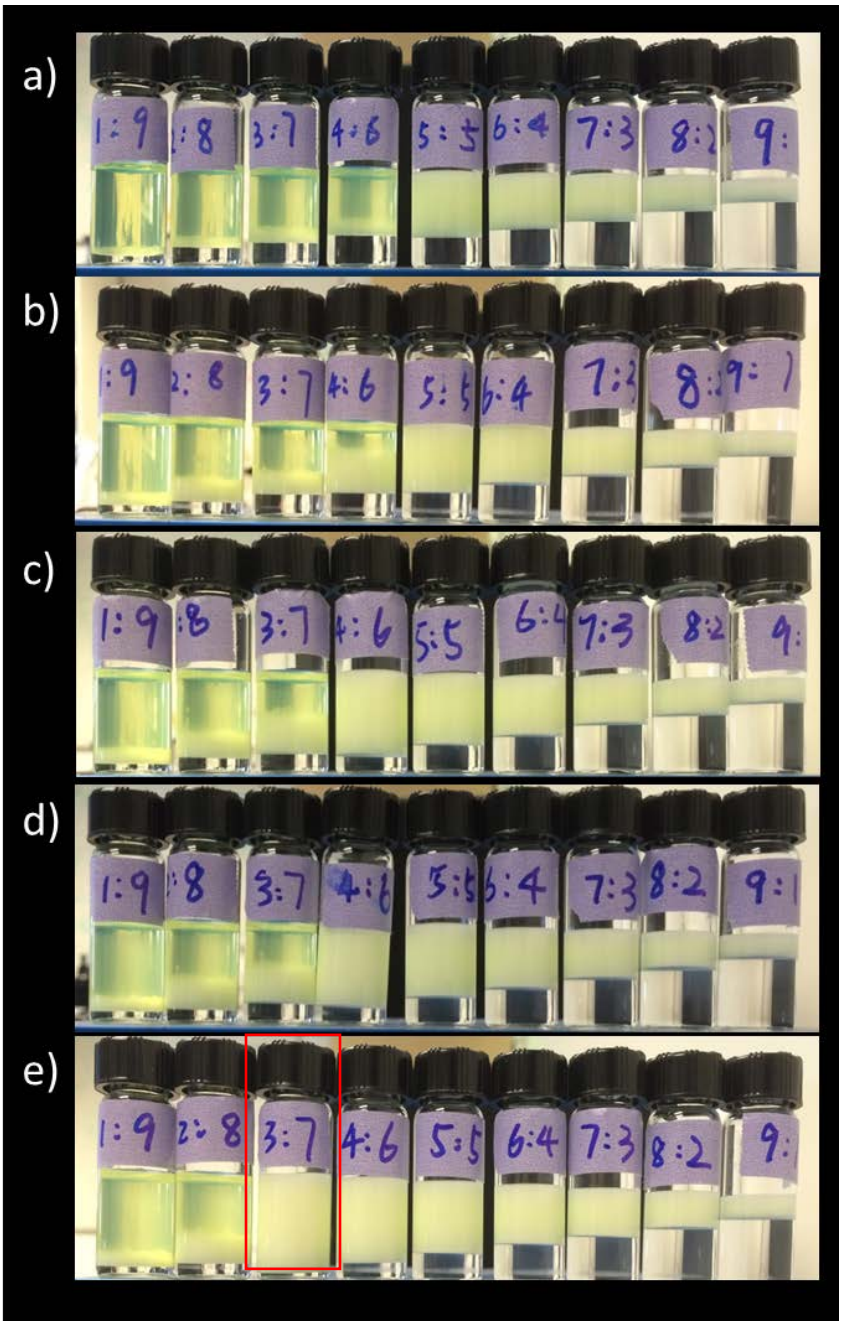

Figure 42. Phase scans. From left to right, the oil to water ratio descends as labeled on the vials. Surfactant concentrations were 0.1%, 0.2%, 0.3%, 0.4%, 0.5% for row a), b), c), d), e), respectively. Pictures were taken after samples had been set still for 1 week. A Winsor IV type emulsion (marked as red in picture) was chosen to make the fracturing fluids.

A gel based fracturing fluid was formulated according to the formula mentioned in previous section. The gel based fracturing fluid consists of 2000-6000 mg/L Hydroxypropyl Guar Gum (HPGG), 2000-10000 mg/L organoboron crosslinker, 1000-10000 mg/L breaker (ammonium persulfate) and 500-1000 mg/L high temperature stabilizer (alkyl alkanolamine). Within these compositions, the fracturing fluid can quickly form a gel at 40 to 100℃ by mixing. After that, the above single phase micro emulsions were mixed into this gel based fracturing fluid in a 1:9 weight ratio and used for later tests.

Interfacial tension (IFT) between the diesel oil phase and aqueous phase under influence of blended surfactants was measured with spinning drop method. The IFT profile shows in Figure 43 that Triton-X/n-butanol reaches its critical micelle concentration at 0.2 w/w% surfactant concentration, which was consistent with emulsion phase study results shown in Figure 41 and Figure 42.

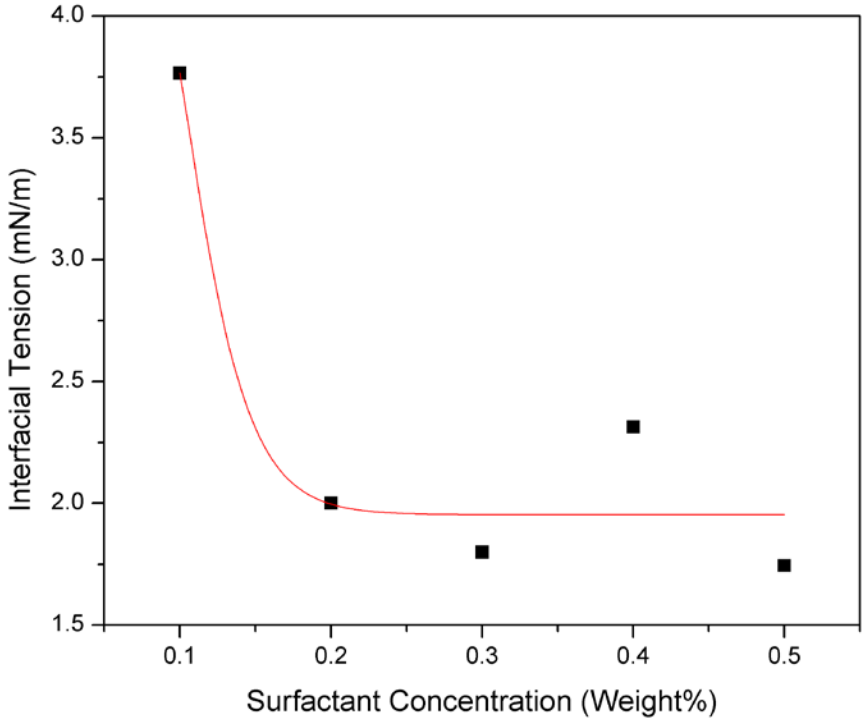

Figure 43. Interfacial tension between the diesel oil and water interface with different concentrations of surfactants. The red line represents the fitted result with lognormal model. Four right data points, 0.2%, 0.3%, 0.4%, 0.5% respectively, showed interfatial tension reached a interfacial tension pleateu. Thus we conclude the concentration of surfactant already reached their critical micelle concentration (CMC)

A.3.2. Compatible Breaker System

The gel breaking time can be controllable by adding different amount of breakers. Depending on the amount of breaker, it usually takes 60 to 120 minutes for the breaking process to complete. Ammonium persulfate and encapsulated breaker OB-1 were both tested to be compatible with our fracturing system.

A.3.3. Rheological Characterization

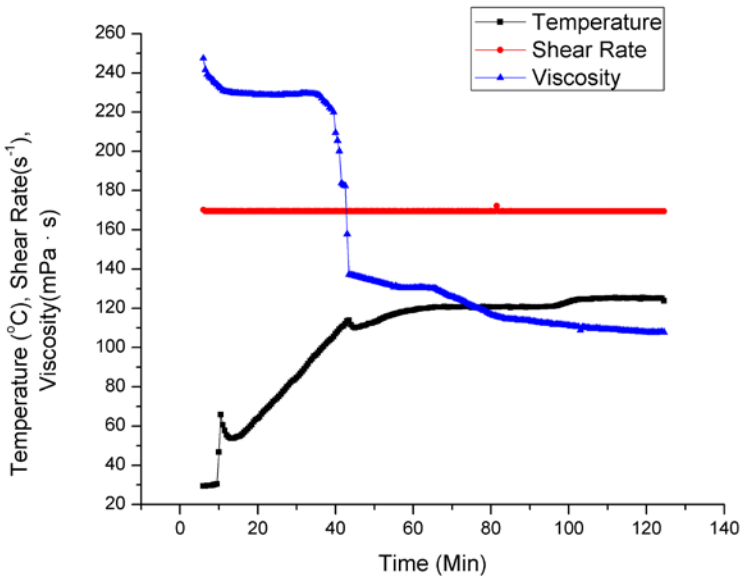

Figure 44. Rheological change of the micro-emulsion fracturing fluid under 120 ºC and 170s^{-1} shearing rate.

Rheological property is tested with rheometer (HAAKE RheoStress 600). To simulate shearing force induced by underground formation, the shear rate is set at 170s^{-1}. Meanwhile, we introduced a gradual temperature increase to simulate the temperature increase caused by friction. As shown in Figure 44, fracturing fluid was sheared under a 170s^{-1} shearing rate and temperature was gradually increased to 120 ºC at 5 ºC /min increasing rate, the fracturing system can still maintain a viscosity above 100mPa•S for more than 2 hours. Our micro-emulsion fracturing fluid exhibited an excellent anti-shear property under high temperature.

A.3.4. Fluid Loss

To evaluate fluid loss caused by the micro-emulsion fracturing fluids comparing with conventional fracturing system, we measured leakoffs of different fracturing fluid formulas with different micro-emulsion percentages. Synthetic 500 PSI (3.5 MPa) differential pressure is applied on the two sides of filtration cell. Volume of fluid that flows out is also measured. Temperature was controlled at 90 ºC during the tests. Applied pressure lasted 36 minutes. Experiment results were plotted in Figure 45.

Synthetic core samples with same composition of Sulige Eastern formation were used in these experiments.

Result showed that a concentration of 5 % or above of micro-emulsion can significantly reduce fluid loss. Change between 5% and 10% was apparent, but subtle, which still can justify our choice to use 10% concentration of micro-emulsions in the whole fracturing fluid.

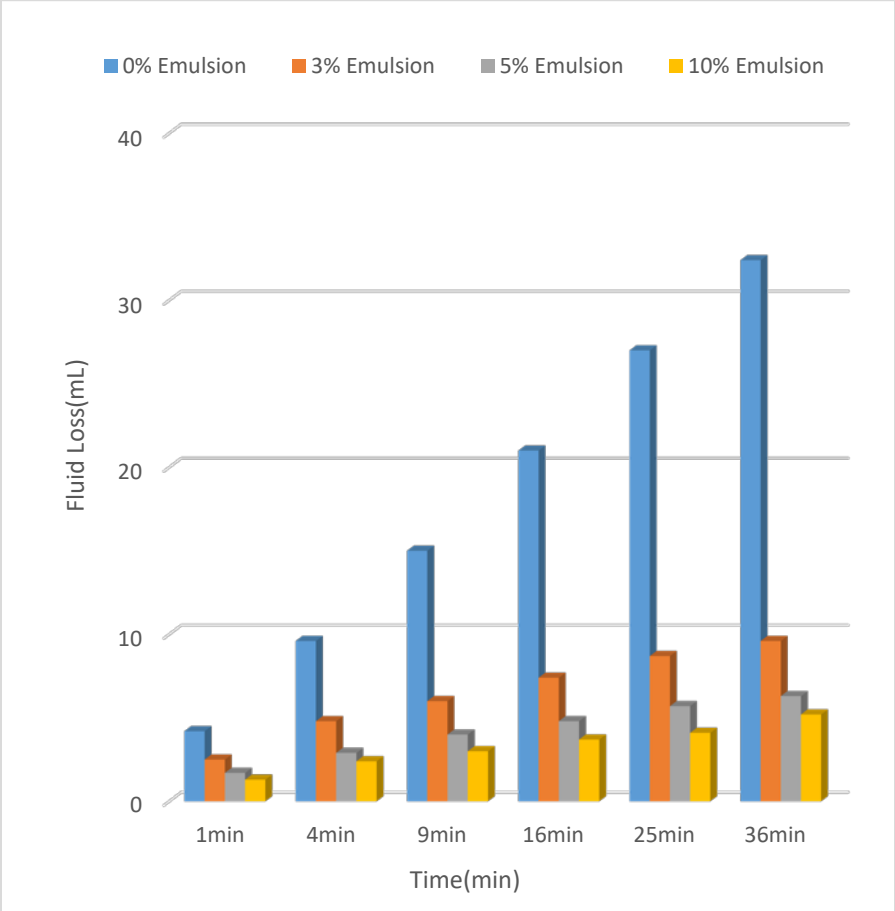

Figure 45. Fluid loss for different fracturing fluid fomulas with different micro-emulsin percentages.

A.3.5. Formation damage test

The core permeability can be calculated with Darcy–Weisbach equation,

$$K = \frac{Q \cdot \mu \cdot L}{\Delta P \cdot A}$$

Where K is sample permeability, μm^2, Q is flow rate, mL/s, L is core sample length, cm, A is core sectional area, cm^2, ΔP is pressure difference, MPa, and μ is fluid viscosity, mPa·s.

Formation damage can be characterized by the percentage of permeability reduction:

$$\eta = \frac{K_1 - K_2}{K_1} \times 100\%$$

,

where K_1 is the permeability before fracturing fluid flooding, and K_2 is the permeability after fracturing fluid flooding.

Experiments were conducted under 120 ^oC, result show as table 1. Data showed that the conventional guar gel fracturing fluid decreases formation permeability by 57.9%, however, our micro-emulsion fracturing fluid only decreased permeability by 16.4%, hence we conclude that micro-emulsion fracturing fluids only caused marginal changes on permeability comparing to the conventional guar gel fracturing fluid.

Table 2 Formation Damage Test Data

Type	Core Sample #	Length (cm)	Diameter (cm)	Porosity (%)	Permeability before test (μm^2)	Permeability after test （μm^2）	Formation damage%
Guar Gel Frac	1#	4.91	2.54	14.59	1.469×10^{-3}	0.619×10^{-3}	57.9
Micro Emulsion Frac	2#	5.73	2.54	14.6	2.647×10^{-3}	2.212×10^{-3}	16.4

A.3.6. Tube Friction Test

Tube friction test was carried out by a coiled tubing system. The total length of the coil was 3 meters. We used two different inner diameter tubes, 0.46 cm and 1.01cm, respectively. The micro-emulsion fracturing fluids formulated according to previous paragraph were then injected. Also we tested the fluids under two different temperatures, 40 ^oC and 80 ^oC, respectively. Results showed in Figure 46Figure 46. The purpose of these experiments is to provide friction reference data for later field applications.

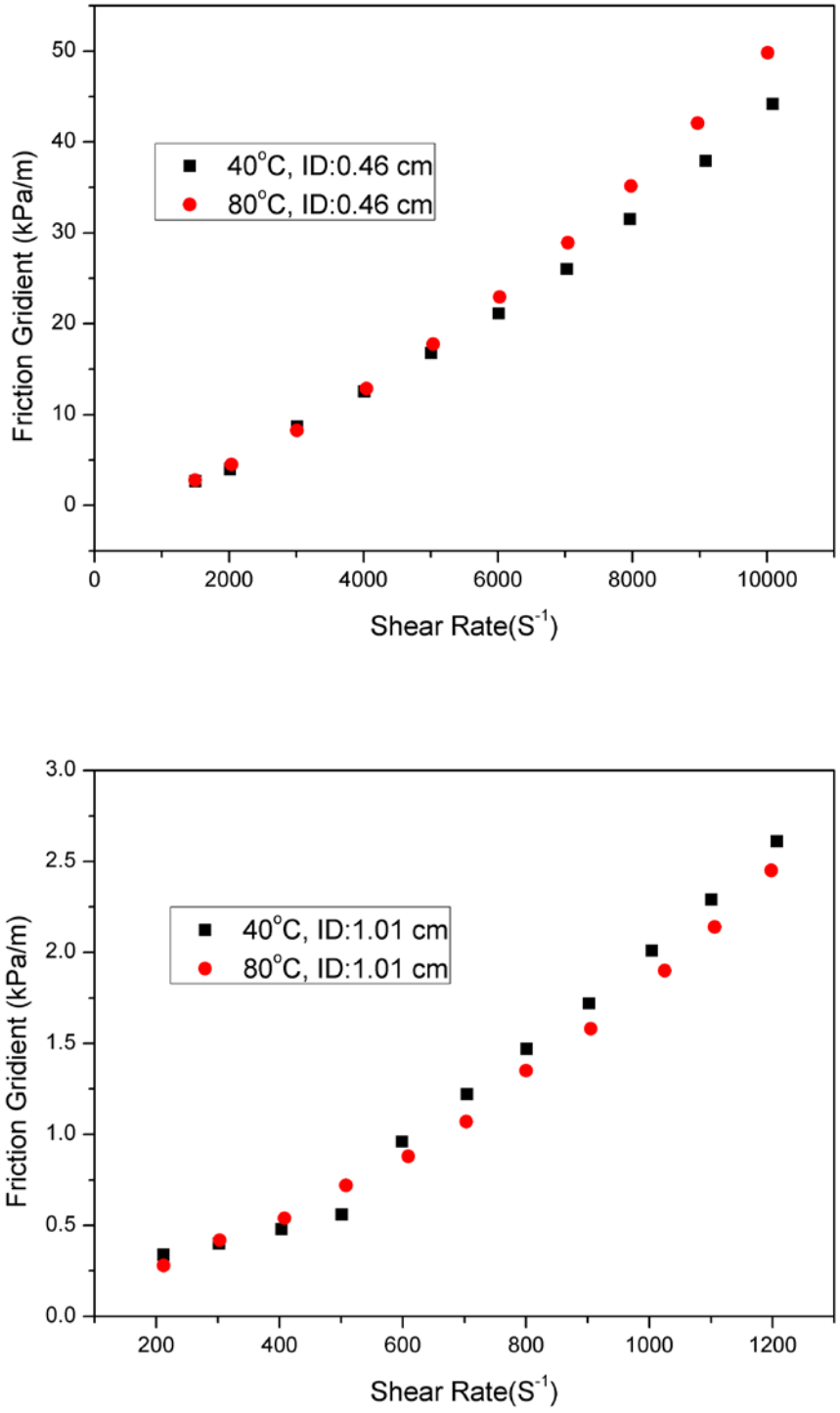

Figure 46. Tube friction profiles with 0.46cm, 1.01cm tubings, under 40°C and 80 °C.

A.4. Conclusion

To solve the fluid loss and formation damage problems in gas reservoirs, we developed a micro-emulsion based fracturing fluids. The ternary phase diagram was used to locate the optimal compositions of the fracturing fluids. After optimizing fluid composition, rheological characterization was measured to access system shear tolerance. The fluid loss and formation damage tests were also carried out to evaluate the fracturing fluids. Results showed that our micro-emulsion fracturing fluids have a robust shear resistance, which ensures a high operation fluid viscosity after pumping down fluid into formation. In addition, our micro-emulsion fracturing fluids caused less fluid loss and formation damage comparing to conventional guar gum fracturing fluids. Compatible breaker system was suggested here for consideration in field implementation. Tube friction profile was measured to provide a reference for field applications. The intrinsic properties of micro-emulsions and micro-emulsion fracturing fluids make them promising tools for economy fracturing operation with increased production lifetime.